

Wordcount: 10386 words

1 1
2
3 2 **Exploring Copula-based Bayesian Model Averaging with multiple**
4
5
6 3 **ANNs for PM_{2.5} ensemble forecasts**
7
8
9 4

10
11 5 Yanlai Zhou^{1,2}, Fi-John Chang¹, Hua Chen³, Hong Li²
12
13

14 6 ¹ Department of Bioenvironmental Systems Engineering, National Taiwan University,
15
16
17 7 Taipei, 10617, Taiwan.
18
19

20 8 ² Department of Geosciences, University of Oslo, P.O. Box 1047 Blindern, N-0316
21
22
23 9 Oslo, Norway.
24

25 10 ³ State Key Laboratory of Water Resources and Hydropower Engineering Science,
26
27
28 11 Wuhan University, Wuhan, 430072, China.
29
30

31 12 **Correspondence author:* Fi-John Chang (changfj@ntu.edu.tw); Yanlai Zhou
32
33
34 13 (yanlai.zhou@whu.edu.cn).
35
36
37
38
39
40
41
42
43
44
45
46
47
48
49
50
51
52
53
54
55
56
57
58
59
60
61
62
63
64
65

Abstract

Quantifying predictive uncertainty of ensemble air quality forecast is very crucial and challenging. This study integrated a Copula-based Bayesian Model Averaging (CBMA) and multiple deterministic artificial neural networks (ANNs) to make accurate ensemble probabilistic $PM_{2.5}$ forecasts. The new approach (CBMA), has a flexible structure that grants the posterior distribution to have any shape owing to the Copula function. The CBMA approach could remove the data transformation and bias correction procedures as it is done in the original BMA, which was taken as the benchmark. The air quality in Taipei City of Taiwan was selected as a study case to evaluate the applicability and reliability of the proposed approach. Three kinds of air quality monitoring stations denoted heavy traffic loads, intensive commercial trading and human intervention, and a natural circumstance with fewer human activities respectively. The forecasts of $PM_{2.5}$ concentrations were regarded as a math function involving meteorological and air quality variables, using long-term (2010-2018) hourly observational datasets. Firstly, four deterministic ANN models were established and evaluated to provide inputs for ensemble forecasting. Then, the two post-processing techniques (i.e. CBMA and BMA) were employed to produce ensemble probabilistic forecasts based on the forecasts obtained from multiple ANN models. The results demonstrated that the CBMA not only could outperform the BMA but also could provide a practical and reliable approach as a complement to multiple deterministic ANN models to create ensemble probabilistic forecasts. From horizons $t+1$ up to $t+4$, the CBMA approach could drive up the Containing Ratio (CR) values by 3.12% - 9.58% as well as reduce the average Relative Band-width (RB) values by 8.63% - 34.48% and the Continuous Ranked Probability Score (CRPS)

1 38 values by 7.62% - 32.89%, in comparison with the BMA one. Consequently, the
2
3 39 predictive uncertainty could be alleviated while model reliability and PM_{2.5} forecast
4
5 40 accuracy could be considerably increased.
6
7

8 41 **Keywords:** Air quality; Ensemble forecast; Uncertainty; Bayesian Model Averaging
9
10 42 (BMA); Copula function
11
12

13 43

14 44 **1. Introduction**

15
16 45 Suspended atmospheric particulate matter (e.g. PM_{2.5}, aerodynamic diameter less than
17
18 46 2.5 µm) is one of main air pollutants (Huang et al., 2014; Zhang et al., 2018). Natural
19
20 47 sources and anthropogenic sources transformation of precursor emissions in the
21
22 48 atmosphere such as SO₂ to Sulphates and NO_x to Nitrates may also cause PM_{2.5}
23
24 49 (Berardis and Eleonora, 2017; Van Fan et al., 2018). The electricity generation
25
26 50 process using overmuch fossil fuels would produce plenty of precursor emissions and
27
28 51 trigger air pollution. The accurate and reliable air quality predictions can provide
29
30 52 technical guidelines for the trade-off between fossil fuels energy and renewable
31
32 53 energy outputs toward cleaner production. Air quality predictions and environmental
33
34 54 impacts of the electricity generation process not only increase efficiencies in the uses
35
36 55 of energy but also are in the interest of cleaner production in power industries (Han et
37
38 56 al., 2019). It is essential to make accurate and reliable air quality forecasts in advance
39
40 57 to mitigate environmental impacts and health risks. There is a noticeably growing
41
42 58 trend to move away from purely deterministic air quality forecasting to probabilistic
43
44 59 air quality forecasting (Krapu and Borsuk, 2019; Zhang, 2017; Zhai and Chen, 2018).
45
46
47
48
49
50
51
52
53
54
55
56
57
58
59
60
61
62
63
64
65

60 Some promising techniques (Table 1) have been used to quantify uncertainties in air
61 quality forecasts, for instance, (1) pre-processing techniques: Fuzzy Clustering (FC)
62 method, Wavelet Transform (WT) and bias-correction method (Dunea et al., 2015;
63 Feng et al., 2015; Gong and Ordieres, 2016; Lohani et al., 2014; Lyu et al., 2017;
64 Monteiro et al., 2013) and (2) post-processing techniques: Multiple Linear Regression
65 (MLR), Kalman filtering, Generalized Likelihood Uncertainty Estimation (GLUE),
66 Bayesian Uncertainty Processor (BUP) and Bayesian Model Averaging (BMA)
67 (Aznarte, 2017; Djalalova et al., 2015; Garner and Thompson, 2013; Kaminska, 2018;
68 Pucer et al., 2018; Zhai and Chen, 2018). Ensemble forecasting techniques are
69 commonly used to characterize diverse uncertainties in air quality forecasts (Bai et al.,
70 2018; Thielen-del and Bruen, 2019). According to the comparative analysis for
71 various probabilistic forecasting techniques (Table 1), the BMA, as one of the smart
72 post-processing methods, employed for weather firstly forecasting, is being broadened
73 to air quality modeling applications, which exhibits ensemble forecasts' advantage
74 (Herr and Krzysztofowicz, 2015; Pucer et al., 2018; Krapu and Borsuk, 2019).
75 Ensemble forecasts with post-processing techniques are commonly used to
76 supplement the information provided by point-value deterministic predictions.
77 Modular design, ensemble modeling and hybridization with deterministic models are
78 yielding new tools for probabilistic air quality forecasting (Liu et al., 2019).

Table 1 Comparison analysis of probabilistic forecasting methods

Methods	Categories	Pros	Cons
Pre-processing	Fuzzy Clustering (FC)	Quantifying the input uncertainty possessing <i>fuzzy characteristics</i>	Only for the input uncertainty possessing
	Wavelet Transform (WT)	Quantifying the input uncertainty possessing <i>periodic or seasonal</i>	a specific characteristic, not for

		<i>characteristics</i>	model structure and parameters uncertainty
	Bias-correction	Quantifying the input uncertainty possessing <i>systematic bias error</i>	
Post-processing	Multiple Linear Regression (MLR)	Quantifying the overall predictive uncertainty of model structure and parameters possessing <i>linear features</i>	Only for the uncertainty possessing linear features
	Kalman filtering	Quantifying the overall predictive uncertainty of model structure and parameters possessing <i>systematic bias error</i>	Only for the single-model independently
	Generalized Likelihood Uncertainty Estimation (GLUE)	Quantifying the overall predictive uncertainty of model structure and parameters possessing <i>nonlinear features</i>	Only for the single-model independently
	Bayesian Uncertainty Processor (BUP)	Quantifying the overall predictive uncertainty of model structure and parameters possessing <i>Gaussian features</i>	Only for the single-model independently and meeting Gaussian assumption
	Bayesian Model Averaging (BMA)	Quantifying the overall predictive uncertainty of <i>multi-model structure and parameters</i>	Only for the specific form of posterior distributions

80 Any ensemble forecast approach relies upon model diversity that different models
81 produce, with specific emphasis and different aspects of the features they want to
82 model (Li et al., 2013; Raftery et al., 2005). Artificial Neural Networks (ANNs) used
83 as data-driven methods to model air quality and meteorological systems have evolved
84 rapidly over the last few decades (Ryan, 2016; Shen et al., 2018). For instance, the
85 Back Propagation Neural Networks (BPNN), the Adaptive Neural Fuzzy Inference
86 System (ANFIS), the Random Forest (RF), the Quantile Regression Neural Networks
87 (QRNN), the Radial Basis Function (RBF), the Extreme Learning Machine (ELM),
88 the Non-linear AutoRegressive with eXogenous inputs neural network (NARX), the
89 Support Vector Machine (SVM) and the Long-Short Term Memory (LSTM) have
90 been widely used to model air quality and meteorological forecasts (e.g. Akbari et al.,

1 91 2018; Ausati and Amanollahi, 2016; Cannon, 2011; Chang et al., 2016; Gao et al.,
2
3
4 92 2018; Nieto et al., 2018; Prasad et al., 2016; Taghavifar et al., 2016; Voukantsis et al.,
5
6 93 2011; Yeganeh et al., 2018; Yu et al., 2016; Zhu et al., 2018; Zhou et al., 2019 a,b).
7
8
9 94 The factors of geographical location, meteorological conditions, population, traffic
10
11 95 density and industrial activities have an impact on the physical-chemical composition
12
13 96 and the concentration of airborne particles (e.g. Fanizza et al., 2018; Li et al., 2018;
14
15 97 Sun et al., 2016; Yu and Stuart, 2017). The mass concentration of atmospheric
16
17 98 particulate matter (e.g. PM_{2.5}) relies on a series of natural and anthropogenic
18
19 99 processes, furthermore, the main contribution stems from secondary particles (Lin and
20
21 100 Zhu, 2018; Lyu et al., 2016; Wu et al., 2018). Secondary particles' formation is
22
23 101 attributed to a lot of factors: ozone, carbon monoxide, carbon dioxide, organic carbon,
24
25 102 sulphur dioxide, nitrogen oxides and meteorological environments like temperature,
26
27 103 precipitation, wind speed and direction as well as relative ambient humidity (Berardis
28
29 104 and Eleonora, 2017; Coelho et al., 2014). Moreover, ensemble forecasting provides a
30
31 105 practical and reliable approach that serves as a complement to ANN models for
32
33 106 simulating and understanding of particle formation, transport, transformation and
34
35 107 deposition mechanisms in the primary, secondary and natural sources and processes
36
37 108 (Chen et al., 2018). Hence, it is interesting to make an in-depth study on ANN models
38
39 109 for improving forecast reliability and accuracy and on the conversion of the
40
41 110 deterministic forecasts into probabilistic forecasts using post-processing ensemble
42
43 111 techniques.

54
55
56
57
58 112 Predictive uncertainties are closely associated with the spatial discretization of
59
60
61
62
63
64
65

1 113 physical processes, model structure and parameterization. Because any air quality
2
3 114 model is considered the brief conceptualization of complicated chemical-physical
4
5
6 115 processes in the atmospheric system, the hypotheses in the conceptual model induce
7
8
9 116 air quality forecasts to get inaccurate. To decrease model uncertainty, the model
10
11
12 117 averaging method is commonly adopted to integrate an ensemble of multiple models
13
14
15 118 by using a linear sum of diverse models. Such model-averaging approaches bring
16
17
18 119 deterministic outputs' linear average and make a combined single-value, for instance,
19
20
21 120 equal weights averaging, MLR, Akaike Information Criterion (AIC) or Bayesian
22
23 121 Information Criterion (BIC)-based model averaging (Breiman and Friedman, 1997;
24
25 122 Buckland et al., 1997; Granger and Ramanathan, 1984; Leslie and Holland, 1991).
26
27
28 123 Even if these model averaging methods have achieved good practicality and
29
30
31 124 applicability, some researchers (e.g. Hoeting et al., 1999; Raftery et al., 2005)
32
33
34 125 contended that the weights cannot thoroughly characterize single models' contribution
35
36
37 126 and advocated BMA's application. The BMA approach can integrate the Probability
38
39
40 127 Density Function (PDF) of different model predictions by means of making a
41
42
43 128 weighted one. The applications of BMA approach in meteorological forecasts
44
45
46 129 motivated its several usages in air quality forecasts (e.g. Mok et al., 2018; Pucer et al.,
47
48
49 130 2018; Pannullo et al., 2016; Weber et al., 2016). However, the conditional PDF in
50
51
52 131 standard BMA is supposed to conform to a Gaussian distribution (Raftery et al., 2005),
53
54
55 132 which is appropriate for some specific predicted variables (e.g. atmospheric pressure
56
57
58 133 and temperature). For other variables (e.g. $PM_{2.5}$, PM_{10} , Ozone, precipitation and
59
60
61 134 wind speed), the Gaussian distribution would be a bad choice, whereas other PDF

1 135 distributions (e.g. Gamma, Gumbel, Pearson type III, Generalized Extreme Value, etc)
2
3 136 would be good choices for fitting predicted variables (Mok et al., 2018; Pucer et al.,
4
5
6 137 2018). Additionally, the standard BMA application need transform the model outputs
7
8
9 138 (or predicted variables) from original space to the Gaussian space. To prevent such
10
11
12 139 information loss during data space transformation, multivariate Copula functions have
13
14
15 140 been used in meteorological and hydrological fields (e.g. Chen and Guo, 2019;
16
17 141 Khajehei and Moradkhani, 2017; Nelsen, 2006; Zhang and Singh, 2019), owing to
18
19
20 142 their outstanding capability of modeling the nonlinear dependence of multiple
21
22
23 143 variables and their allowance of some flexibility in choosing an arbitrary marginal
24
25
26 144 distribution. In a study by Madadgar and Moradkhani (2014), the combination of
27
28 145 multivariate Copula function and BMA (CBMA) can relax the Gaussian assumption
29
30
31 146 of PDFs. The CBMA approach showed superior practicality and reliability in
32
33
34 147 hydrologic forecasts (e.g. rainfall-runoff processes). Whereas the review of the
35
36
37 148 available literature indicates the CBMA has not been applied in air quality forecasts.
38
39
40 149 Consequently, it is imminent to implement an in-depth study on the exploration of
41
42
43 150 CBMA for quantifying and reducing the uncertainty encountered in ensemble air
44
45
46 151 quality forecasts.

47
48 152 The research gaps and how did this work fulfill research gaps were described as
49
50
51 153 follows. First, the current ensemble models for air quality forecasting mainly involved
52
53
54 154 single-output ANNs and/or shallow learning ANNs whereas multi-output ANNs and
55
56
57 155 deep learning ANNs were rarely applied in the ensemble forecast of air quality.
58
59
60 156 Accordingly, the integration of the single-output, the multi-output, the shallow

1 157 learning, and the deep learning ANN models were proposed to configure the four
2
3 158 members of the ensemble scheme for air quality forecasting (i.e. point forecasts).
4
5
6 159 Second, the contribution of this study was attributed to exploring and extending our
7
8
9 160 previous works (i.e. deterministic ANN models) (Zhou et al., 2019a,b) for making
10
11 161 probabilistic ensemble $PM_{2.5}$ forecasts. Third, the family of Bayesian ensemble
12
13
14 162 forecast methods consists of BMA and CBMA. The BMA method has been widely
15
16
17 163 adopted for air quality forecasting. Despite the CBMA is an existing method, it has
18
19
20 164 been rarely employed in the air quality forecast field. Accordingly, the CBMA
21
22
23 165 method was introduced to create a probabilistic ensemble scheme for air quality
24
25
26 166 forecasting based on point forecasts driven by multiple ANNs.

27
28 167 The novelties of this study relied on: multiple ANNs with various characteristics
29
30
31 168 were for the first time integrated into a novel ensemble scheme for air quality
32
33
34 169 forecasting while the combination of Copula function and BMA (CBMA) was taken
35
36
37 170 as an existing method but rarely used in the air quality forecast field.

38
39 171 In this study, a CBMA-based approach was proposed for integrating CBMA and
40
41
42 172 multiple ANNs to reduce the prediction intervals of ensemble $PM_{2.5}$ forecasts. Firstly,
43
44
45 173 multiple ANN models were constructed for creating deterministic $PM_{2.5}$ forecasts
46
47
48 174 independently. Then for comparison purpose, the CBMA approach and the BMA
49
50
51 175 approach were implemented to transform the deterministic $PM_{2.5}$ forecasts of multiple
52
53
54 176 ANN models into the ensemble probabilistic $PM_{2.5}$ forecasts respectively. The
55
56
57 177 regional $PM_{2.5}$ forecasts in Taipei City of Taiwan were taken as a study case to assess
58
59
60 178 the applicability as well as reliability of the proposed ensemble forecast method.

1 179

2
3
4 180 **2. Methods**

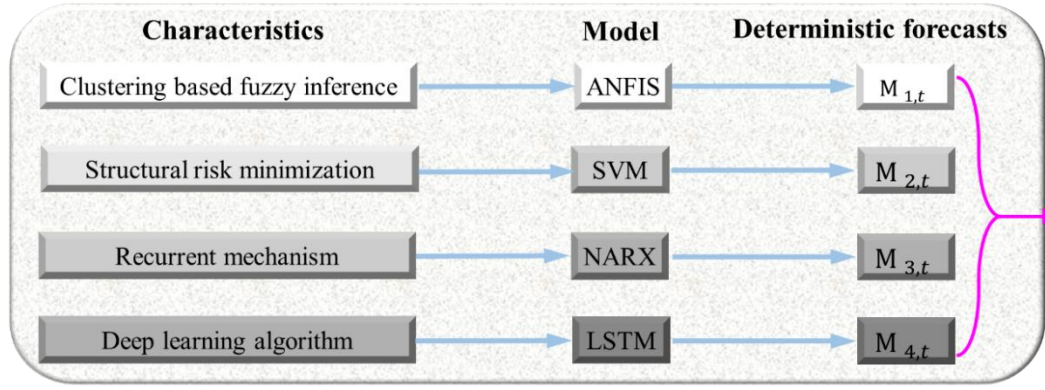
5
6 181 Figure 1 illustrated the ensemble forecast architecture that integrated the four
7
8
9 182 deterministic ANN models (Figure 1 (a)) with the BMA (Figure 1 (b)) or the CBMA
10
11 183 ensemble forecast approach (Figure 1 (c)). The deterministic point forecasts were
12
13
14 184 created by multiple ANN models independently. The ensemble forecast could be
15
16
17 185 improved by CBMA, as compared with the benchmark method (i.e. BMA). The used
18
19
20 186 methods were briefly described as below.

21
22
23 187 *2.1 Deterministic ANN models*

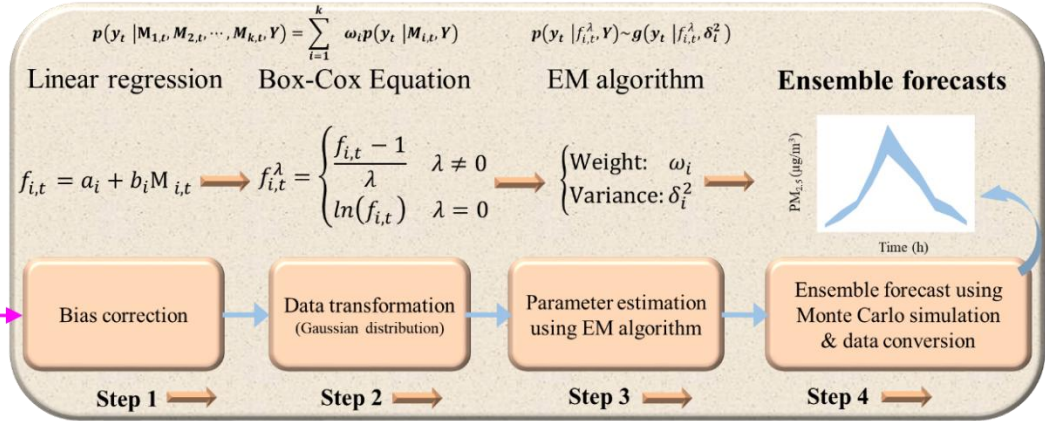
24
25 188 In this study, the selected ensemble members included single-output ANFIS
26
27
28 189 (S-ANFIS) (Jang, 1993), multi-output SVM (M-SVM) (Xu et al., 2013; Zhou et al.,
29
30
31 190 2019a), single-output NARX (S-NARX) (Leontaritis and Billings, 1985) and
32
33
34 191 multi-output deep learning LSTM (M-LSTM) (Zhou et al., 2019b) models. All models
35
36
37 192 were the artificial neural network models and constructed for deterministic PM_{2.5}
38
39
40 193 forecasting. The models have the same network structures (i.e. input layer, hidden
41
42 194 layer & output layer) whereas the models have different machine learning
43
44
45 195 mechanisms. The S-ANFIS can extract the static and fuzzy feature between air quality
46
47
48 196 and other factors, the M- SVM can extract the non-linear relationship between them,
49
50
51 197 the S-NARX can extract dynamic feature between them, while the M-LSTM can
52
53
54 198 extract the long and short-term relationship between them.

1
2
3
4
5
6
7
8
9
10
11
12
13
14
15
16
17
18
19
20
21
22
23
24
25
26
27
28
29
30
31
32
33
34
35
36
37
38
39
40
41
42
43
44
45
46
47
48
49
50
51
52
53
54
55
56
57
58
59
60
61
62
63
64
65

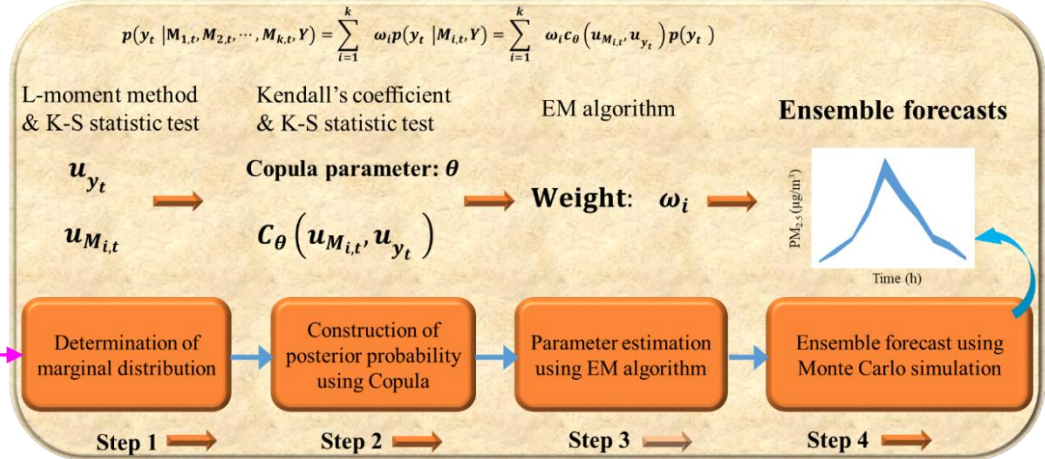
a. ANN models



b. BMA



c. CBMA



$M_{i,t}$ $f_{i,t}$ Y_t Y are the i th model forecast, i th bias-corrected forecast, ensemble forecast variable at the t time and training data.

$p(y_t | M_{i,t}, Y)$ $p(y_t)$ are the posterior density function of y , given model forecast $M_{i,t}$, and training data Y , and probability density function of y .

a_i b_i λ $f_{i,t}^\lambda$ are the i th coefficients (a, b) of linear regression, Box-Cox coefficient, and i th transformed bias-corrected forecast at the t time.

ω_i δ_i^2 θ k are the weight coefficient and variance of i th model forecast, Copula function parameter, and the number of ensemble models.

$u_{M_{i,t}}$ u_{y_t} $C_\theta(\cdot, \cdot)$ are the marginal distributions of model forecast and ensemble forecast variable, and Copula function.

199
200 **Figure. 1** Ensemble probabilistic forecast architecture. (a) ANN models. (b) Bayesian
201 Model Averaging (BMA). (c) Copula-based Bayesian Model Averaging (CBMA) for
202 ensemble forecasting.

1 203 In the case of static ANNs (i.e. S-ANFIS and M-SVM), a typical three-layered
2
3 204 static feedforward neural network, which is comprised of multiple elements including
4
5
6 205 nodes and weight connections that link nodes. In the case of recurrent ANNs (i.e.
7
8
9 206 S-NARX and M-LSTM), the recurrent neural network involves three layers and
10
11 207 constitutes recurrent connections from the outputs, which can delay several unit times
12
13 208 to produce new inputs. More detailed descriptions of the four models and their
14
15 209 parameters setting for air quality forecasting can be found in the references (Ausati
16
17 210 and Amanollahi, 2016; Ghazi and Khadir, 2009; Prasad et al., 2016; Zhou et al., 2019
18
19
20
21
22 211 a,b).

25 212 Air quality data with specific time-lags (e.g. PM_{2.5}, PM₁₀, ozone, oxynitride,
26
27 213 nitrogen dioxide, nitric oxide, sulfur dioxide, carbon monoxide, etc) and
28
29
30 214 meteorological data with specific time-lags (e.g. precipitation, temperature, wind
31
32
33 215 speed and direction as well as relative humidity) constituted the input variables while
34
35
36 216 multi-step-ahead air quality forecasts (e.g. PM_{2.5} concentration from t+1 up to t+4,
37
38
39 217 horizon = 4) constituted the output variables.

42 218 The differences of four ANN models were summarized as (1) the two models
43
44 219 (S-ANFIS & S-NARX) possessed single-output model structures where the two
45
46
47 220 models (M-SVM & M-LSTM) possessed multi-output model structures; (2) the
48
49
50 221 former three models (i.e. S-ANFIS, M-SVM & S-NARX) were classified as shallow
51
52 222 neural networks (i.e. number of hidden layers = 1) whereas the fourth model (i.e.
53
54
55 223 M-LSTM) was classified as deep learning neural networks (i.e. number of hidden
56
57
58 224 layers ≥ 2); and (3) the former two models (i.e. S-ANFIS & M-SVM) were classified

225 as static (i.e. non-recurrent) neural networks whereas the latter two models (i.e.
 226 S-NARX & M-LSTM) were classified as dynamic (i.e. recurrent) neural networks.
 227 Moreover, the S-ANFIS and S-NARX models need to construct multiple independent
 228 models to output air quality forecast at diverse monitoring stations whereas the
 229 M-SVM and M-LSTM models require only one forecast model to make air quality
 230 multi-outputs. That is to say, the selected four ensemble members can provide model
 231 diversity for the applications of the following ensemble forecast approaches.

232 2.2 Bayesian Model Averaging (BMA)

233 BMA is a post-processing technique used to integrate the forecast results that are
 234 created by different models in virtue of making an ensemble PDF. The predicted
 235 distribution of a realization of the observation y_t , considering the multiple forecasts
 236 of k models $\{M_{1,t}, M_{2,t}, \dots, M_{k,t}\}$, and the observed data Y within the training stage
 237 can be formulated as follows.

$$238 \quad p(y_t | M_{1,t}, M_{2,t}, \dots, M_{k,t}, Y) = \sum_{i=1}^k \omega_i p(y_t | M_{i,t}, Y) \quad (1)$$

239 where $p(y_t | M_{1,t}, M_{2,t}, \dots, M_{k,t}, Y)$ is the predictive distribution of the realization of
 240 the observation y_t , given the independent forecasts of k models $\{M_{1,t}, M_{2,t}, \dots, M_{k,t}\}$,
 241 and the observed data Y . $p(y_t | M_{i,t}, Y)$ is the posterior distribution of function of y_t ,
 242 given model forecast $M_{i,t}$, and training data Y . ω_i is the weight coefficient of i th
 243 model. The general implementation procedure of the BMA approach consisting of
 244 four basic steps can be found in Appendix A.

245 2.3 Copula-based Bayesian Model Averaging (CBMA)

246 From what has been discussed above, the predictive distribution in the BMA approach

1 247 is generally confined to a specific parameter distribution (e.g. Gaussian distribution)
2
3 248 and is computed by a weighted sum of forecast PDFs. Therefore, we clarified a
4
5
6 249 general procedure that fused multivariate Copula function into the original BMA
7
8
9 250 approach (CBMA) to relax the limitations of unbiased forecasts and Gaussian
10
11
12 251 distribution.

13
14 252 Let $u_{M_{i,t}}$ and u_{y_t} be the sampling values in CDFs of U_M and U_y respectively.
15
16
17 253 Let $p_M(u_{M_{i,t}})$ and $p_y(u_{y_t})$ be the Probability Density Functions (PDFs) of the
18
19
20 254 forecast variables of multiple models ($M_{i,t}$) and realization of observation (y_t)
21
22
23 255 respectively. Using the PDF of Copula function, a joint PDF of $(u_{M_{i,t}}, u_{y_t})$ and a
24
25
26 256 conditional probability can be constructed as follows.

$$27 \quad 28 \quad 29 \quad 30 \quad 31 \quad 32 \quad 33 \quad 34 \quad 35 \quad 36 \quad 37 \quad 38 \quad 39 \quad 40 \quad 41 \quad 42 \quad 43 \quad 44 \quad 45 \quad 46 \quad 47 \quad 48 \quad 49 \quad 50 \quad 51 \quad 52 \quad 53 \quad 54 \quad 55 \quad 56 \quad 57 \quad 58 \quad 59 \quad 60 \quad 61 \quad 62 \quad 63 \quad 64 \quad 65$$

$$257 \quad p(u_{M_{i,t}}, u_{y_t}) = c_{\theta_i}(u_{M_{i,t}}, u_{y_t}) \cdot p_M(u_{M_{i,t}}) \cdot p_y(u_{y_t}) \quad (2a)$$

$$258 \quad p(u_{y_t} | u_{M_{i,t}}) = \frac{p(u_{M_{i,t}}, u_{y_t})}{p_M(u_{M_{i,t}})} = c_{\theta_i}(u_{M_{i,t}}, u_{y_t}) \cdot p_y(u_{y_t}) \quad (2b)$$

259 where $p(u_{M_{i,t}}, u_{y_t})$ is the joint PDF of $(u_{M_{i,t}}, u_{y_t})$. $c_{\theta_i}(u_{M_{i,t}}, u_{y_t})$ is the Copula
260 joint PDF of $(u_{M_{i,t}}, u_{y_t})$ and θ_i is the parameter of the Copula function.
261 $p(u_{y_t} | u_{M_{i,t}})$ is the conditional probability of u_{y_t} , given the value of $u_{M_{i,t}}$. Then, the
262 conditional probability (Eq. (2b)) is used to replace the posterior probability (Eq. (1))
263 and the predicted distribution of the realization of observation y_t is updated as
264 follows.

$$265 \quad p(y_t | M_{1,t}, M_{2,t}, \dots, M_{k,t}, Y) = \sum_{i=1}^k \omega_i p(y_t | M_{i,t}, Y) \\ = \sum_{i=1}^k \omega_i c_{\theta_i}(u_{M_{i,t}}, u_{y_t}) \cdot p_y(u_{y_t}) \quad (3)$$

266 As seen in Eq. (3), the posterior distribution $p(y_t | M_{i,t}, Y)$ is directly calculated

267 without needs to use both bias-correction methods (Eq. (1) in Appendix A) and
 268 Gaussian data transformation (Eq. (2) in Appendix A). The general implementation
 269 procedure of the CBMA approach consisting of four basic steps can be found in
 270 Appendix B.

271 It is noted that the differences between BMA approach and CBMA approach
 272 include: (1) the former demands a particular conditional PDFs (e.g. Gaussian), or data
 273 transformation (Non-Gaussian PDFs) and bias-correction for model forecasts whereas
 274 the latter has a flexible structure and relaxes the type of conditional PDFs and (2) the
 275 former needs to estimate the parameters of weight (ω_i) and variance (δ_i^2) whereas the
 276 latter needs to estimate the Copula parameter (θ_i) and the weight (ω_i).

277 The general implementation programming of used machine learning models
 278 (ANFIS, SVM, NARX, LSTM) and Copula function can be obtained from the Statistics
 279 and Machine Learning Toolbox of the Matlab software (website:
 280 <https://ww2.mathworks.cn/products/statistics.html#machine-learning>).

281 *2.4 Evaluation criteria*

282 The Root-Mean-Square Error (RMSE) and the goodness-of-fit with respect to the
 283 benchmark (G_{bench}) were introduced to assess the accuracy of the deterministic
 284 forecast model. The two indicators were defined as follows.

$$285 \quad \text{RMSE} = \sqrt{\frac{1}{T} \sum_{t=1}^T (\hat{Y}(t) - Y(t))^2}, \quad \text{RMSE} \geq 0 \quad (4)$$

$$286 \quad G_{\text{bench}} = \left(1 - \frac{\sum_{i=1}^T (\hat{Y}(t) - Y(t))^2}{\sum_{i=1}^T (Y(t) - Y_{\text{bench}}(t))^2} \right) \times 100\%, \quad G_{\text{bench}} \leq 100\% \quad (5)$$

287 where $\hat{Y}(t)$ and $Y(t)$ are the model forecast and observation at the t -th time,
 288 respectively. $Y_{\text{bench}}(t)$ is the observation moved backwards by n th time lags, for

1 289 instance, for the horizon $t + n$, $Y_{\text{bench}}(t) = Y(t - n)$.

2
3 290 To evaluate the performance of probabilistic forecast models, the Containing
4
5
6 291 Ratio (CR), the average Relative Band-width (RB) and the Continuous Ranked
7
8
9 292 Probability Score (CRPS), were adopted for assessing the goodness of the prediction
10
11
12 293 bounds (Gneiting and Raftery, 2007; Gneiting, 2008; Xiong and O'Connor, 2008).
13
14 294 Their mathematical formulas were described below.

15
16
17 295
$$N(t) = \begin{cases} 1, & \text{if } (q_l(t) \leq \hat{Z}(t) \leq q_u(t)) \\ 0, & \text{else} \end{cases} \quad (6a)$$

18
19
20
21 296
$$CR = \frac{\sum_{t=1}^N N(t)}{N} \times 100\% \quad (6b)$$

22
23
24 297
$$RB = \frac{1}{N} \sum_{t=1}^N \left(\frac{q_u(t) - q_l(t)}{Z(t)} \right) \quad (7)$$

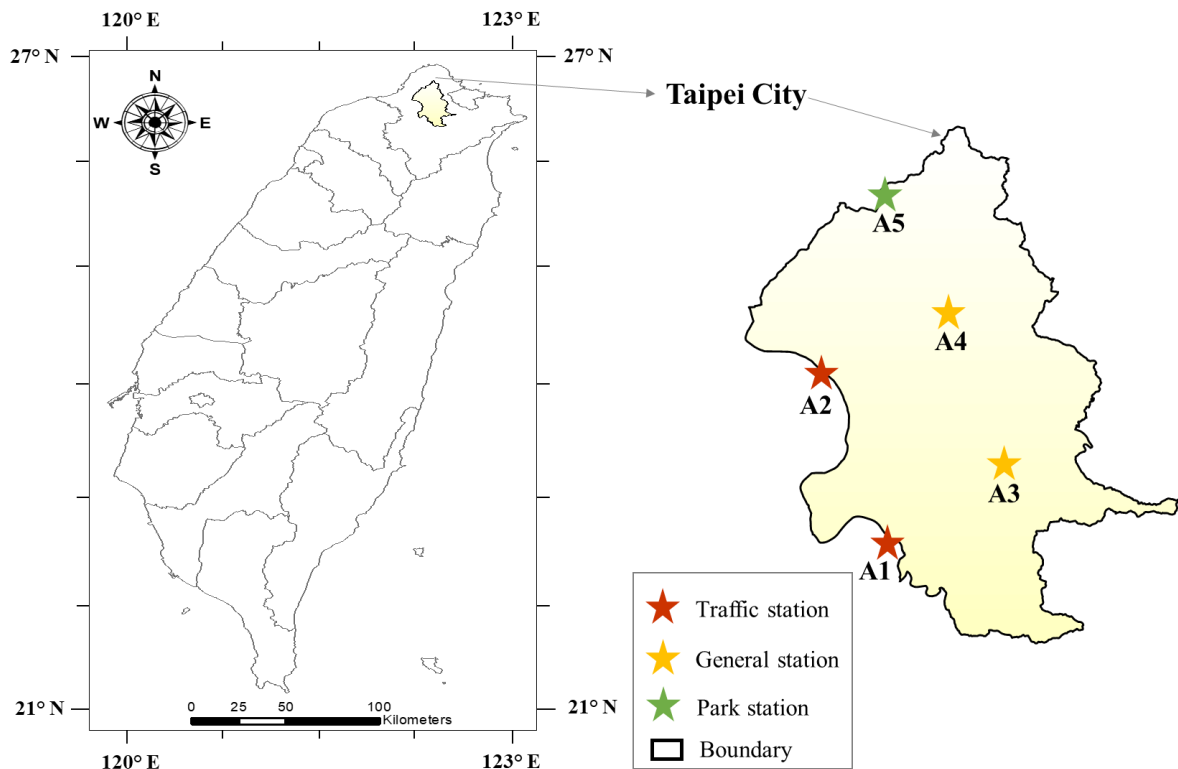
25
26
27 298
$$CRPS = \int_{-\infty}^{+\infty} [F^f(x) - F^o(x)]^2 dx \quad (8)$$

28
29 299 where $q_l(t)$ and $q_u(t)$ are the lower and upper boundaries of the forecasted data
30
31
32 300 corresponding to a given confidence level at the t time respectively. $F^f(x)$ and
33
34
35 301 $F^o(x)$ are the cumulative distribution functions of the forecast and observation
36
37
38 302 distributions, respectively. x is the variable of the cumulative distribution function.
39
40
41 303 The value of $N(t)$ is either 0 or 1, in which 0 indicates the observed data falls
42
43
44 304 outside of its prediction bounds while 1 indicates the observed data falls within its
45
46
47 305 prediction bounds. These evaluation criteria indicate that models with higher G_{bench}
48
49
50 306 and CR values but lower RMSE, RB and CRPS values would produce better
51
52
53 307 performances.

54 308
55
56
57 309 **3. Study area and materials**

58
59
60 310 The study area (Figure 2) was briefly introduced as follows. With the economy and
61
62
63
64
65

1 311 population fast boosting, one of the hot topics in Taiwan focused on air quality
2
3 312 deterioration. People in Taipei City were compelled to handle a high-level
4
5
6 313 intervention of PM_{2.5}. Air pollution not just induced respiratory diseases but also
7
8
9 314 caused a matter of life or death. Hence, it is imperative to make accurate and reliable
10
11
12 315 PM_{2.5} forecasts so as to adequately process the health risk caused by regional air
13
14
15 316 pollution.



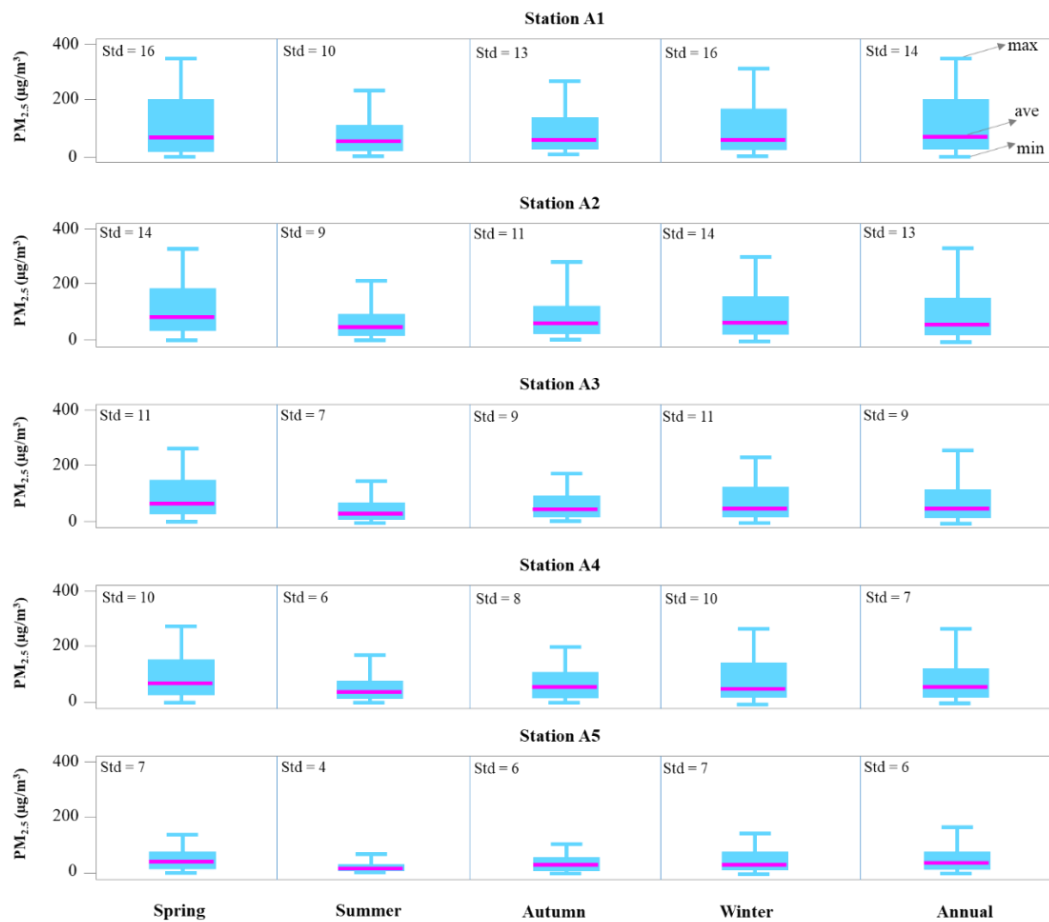
317
318 **Figure. 2** Distribution of air quality monitoring stations (A1-A5) in Taipei City.
319

320 The positions of Taipei City and 5 air quality monitoring stations were presented
321 in Figure 2. Stations A1 (Yonghe) and A2 (Sanchong) where the stations located in
322 areas of heavy traffic are traffic stations, Stations A3 (Songshan) and A4 (Shilin)
323 where the stations located in areas of intensive human activities and commercial
324 trading are general stations, and Station A5 (Yangming) where the station located in
325 the Yang-Ming Park is a park station. The Environmental Protection Administration

1 326 (EPA) in Taiwan (<https://taqm.epa.gov.tw/taqm/en/b0101.aspx>) provided a
2
3 327 convenient open data platform where researchers could get access to many kinds of
4
5
6 328 Taiwan-related data such as air quality and meteorological datasets. Hourly data of
7
8
9 329 air quality factors (eight variables: PM_{2.5}, PM₁₀, ozone, oxynitride, nitrogen dioxide,
10
11
12 330 nitric oxide, sulfur dioxide, carbon monoxide) and meteorological factors (five
13
14
15 331 variables: precipitation, temperature, wind speed and direction as well as relative
16
17
18 332 humidity) over a span of 9 years (2010-2018) were available. A total of 78,888
19
20 333 ($=(2 \times 366) + (7 \times 365) \times 24$) hourly datasets were used in this study, where 35,064 data
21
22
23 334 (4 years) were used for model training while the remaining 26,304 data (3 years) and
24
25
26 335 17,520 data (2 years) were used for model validating and testing respectively. The
27
28
29 336 data standardization that centered the mean to 0 and the standard deviation to 1, was
30
31
32 337 conducted to decrease the negative effect of the different scales of input data on the
33
34
35 338 model's learning ability.

36
37 339 Figure 3 presented the statistic indexes of seasonal and annual PM_{2.5}
38
39 340 concentration at five air quality monitoring stations. We noticed that the statistic
40
41
42 341 indexes of the maximum, average and standard derivation at traffic stations (A1 and
43
44
45 342 A2) were the highest while those in the park station (A5) were the lowest, which
46
47
48 343 could be due to the primary source of particulate matter of a station. Based on the
49
50
51 344 highest values (≥ 0.5) of the Kendall tau coefficients (Maidment, 1993), 1h-4h time
52
53
54 345 lags were identified for air quality factors at traffic stations (A1 and A2) and 1h-2h
55
56
57 346 time lags were identified for air quality factors at general and park stations (A3, A4
58
59 347 and A5) while 1h-4h time lags were identified for meteorological factors at all
60
61
62
63
64
65

348 stations (Zhou et al., 2019 a,b).



349

350 **Figure. 3** Statistic indexes of seasonal $PM_{2.5}$ concentrations from 2010 to 2018 (9
351 years) at five air quality monitoring stations in Taipei City. The abbreviations (max,
352 ave, min, std) denote the maximum, average, minimum and standard deviation
353 respectively.

354

355 4. Results and discussion

356 Both the CBMA approach and the BMA approach were employed to integrate the

357 $PM_{2.5}$ forecasts of four deterministic ANN models and the BMA approach served as a

358 benchmark. The results and findings were presented in the order of the deterministic

359 $PM_{2.5}$ forecasts of four ANN models (Section 4.1), the determination of marginal

360 distributions and the Copula function (Section 4.2), the ensemble $PM_{2.5}$ forecasts and

1 361 the summarization (Section 4.3), shown as follows.

2
3 362 *4.1 Deterministic PM_{2.5} forecasts of four ANN models*

4
5
6 363 The four models (S-ANFIS, M-SVM, S-NARX and M-LSTM) were applied for
7
8
9 364 deterministic forecasting PM_{2.5} concentrations of five monitoring stations (A1-A5)
10
11 365 from horizons t+1 up to t+4 respectively. The RMSE and G_{bench} scores over the testing
12
13 366 stages were calculated for each ANN model (Table 2). The RMSE and G_{bench} scores
14
15 367 indicated that the performance of static models (S-ANFIS & M-SVM) was not as
16
17 368 good as the recurrent models (S-NARX & M-LSTM) at the traffic stations (A1 & A2)
18
19
20 369 and the general stations (A3 & A4). While the single-output modes (S-ANFIS &
21
22 370 S-NARX) performed better than the multi-output models (M-SVM & M-LSTM) at
23
24
25 371 the park station (A5). This was mainly due to the different learning mechanisms (or
26
27 372 model structures) used for the configuration of each model and the simulation of the
28
29
30 373 different air pollutant generating processes. The secondary processes (e.g. stations A1
31
32 374 & A2) and primary processes (e.g. stations A3 & A4) represented complex and
33
34
35 375 indirect air pollutant generating mechanisms and then required complex ANN models
36
37 376 (e.g. S-NARX or M-LSTM) with recurrent or deep learning algorithms (complex
38
39 377 model structure and a large number of parameters) to characterize such processes. The
40
41
42 378 natural processes (e.g. station A5) represented simplex and direct air pollutant
43
44
45 379 generating mechanisms and then only required simplex ANN models (e.g. S-ANFIS
46
47 380 or S-NARX) with single-output structure (simplex mode structure and fewer
48
49
50 381 parameters) to characterize such processes. As a reminder, the multi-model ensemble
51
52
53 382 strategy was a means to exploit the diversity of skillful predictions from different
54
55
56
57
58
59
60
61
62
63
64
65

383 models. Hence, from a perspective of regional air quality forecast accuracy, it needs
 384 an ensemble technique (BMAs) to combine PM_{2.5} forecasts of different deterministic
 385 models and improves their effectiveness for regional air quality forecasts.

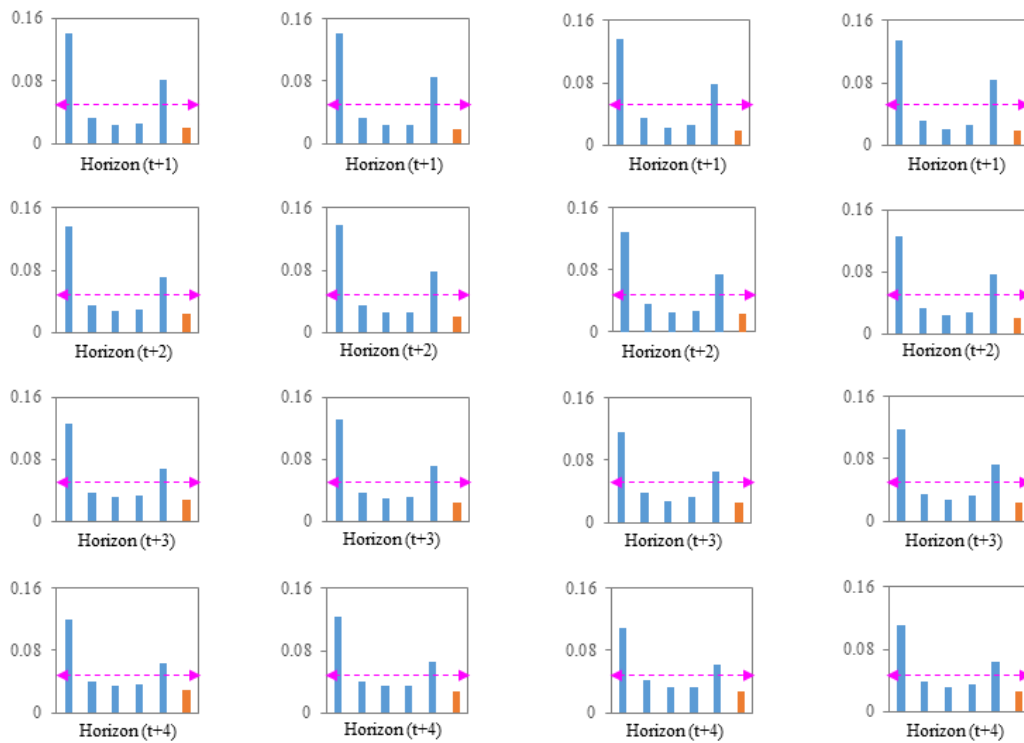
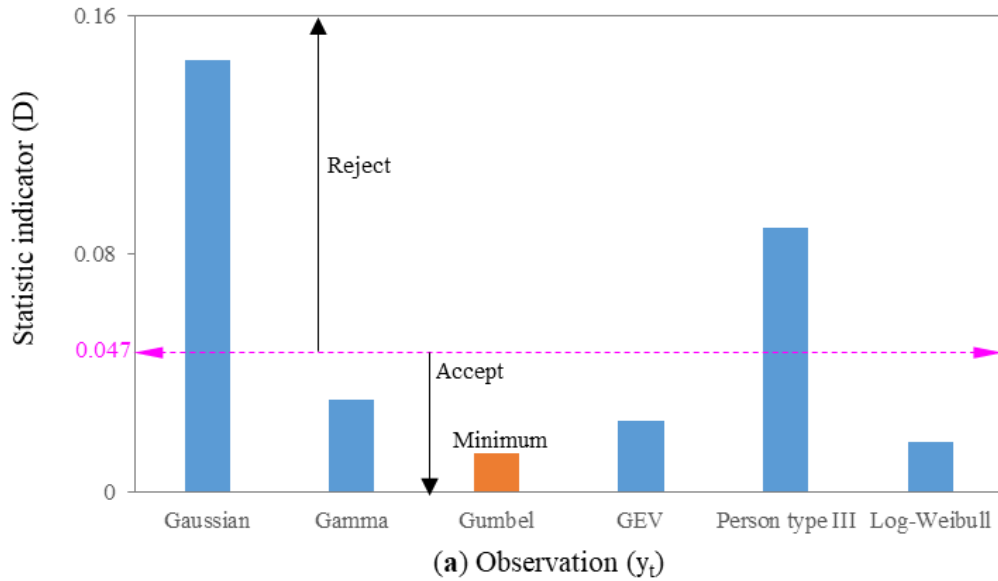
386 **Table 2** Comparison performance of four ANN models for deterministic PM_{2.5}
 387 forecasts from horizons t+1 up to t+4 in the testing stage at different stations.

Station	Horizon	ANFIS		SVM		NARX		LSTM	
		RMSE	G _{bench}	RMSE	G _{bench}	RMSE	G _{bench}	RMSE	G _{bench}
		($\mu\text{g}/\text{m}^3$)		($\mu\text{g}/\text{m}^3$)		($\mu\text{g}/\text{m}^3$)		($\mu\text{g}/\text{m}^3$)	
A1	t+1	4.86	0.92	4.62	0.93	4.51	0.95	4.41	0.95
	t+2	5.77	0.87	5.68	0.90	5.43	0.91	5.11	0.92
	t+3	8.35	0.82	8.09	0.85	7.32	0.86	6.14	0.87
	t+4	11.33	0.78	11.26	0.80	10.78	0.82	9.55	0.84
A2	t+1	4.66	0.91	4.58	0.92	4.47	0.94	4.31	0.95
	t+2	5.33	0.87	5.26	0.88	5.06	0.90	4.83	0.92
	t+3	7.49	0.76	7.34	0.78	7.12	0.82	7.04	0.85
	t+4	10.38	0.71	10.16	0.73	9.94	0.75	9.45	0.77
A3	t+1	4.13	0.92	4.05	0.93	3.88	0.93	3.65	0.94
	t+2	5.23	0.88	5.11	0.90	4.92	0.91	4.71	0.92
	t+3	6.20	0.78	6.13	0.81	6.05	0.83	5.94	0.85
	t+4	9.29	0.72	9.15	0.74	8.67	0.76	8.21	0.78
A4	t+1	3.86	0.90	3.72	0.92	3.61	0.93	3.55	0.94
	t+2	5.04	0.88	4.97	0.90	4.89	0.91	4.72	0.92
	t+3	6.30	0.80	6.21	0.83	6.13	0.86	6.06	0.88
	t+4	8.92	0.73	8.85	0.75	8.66	0.81	8.57	0.83
A5	t+1	2.51	0.91	2.58	0.89	2.12	0.93	2.65	0.88
	t+2	3.61	0.88	3.78	0.86	3.36	0.90	3.90	0.84
	t+3	5.18	0.84	5.57	0.81	5.03	0.87	5.86	0.78
	t+4	7.26	0.78	7.59	0.75	7.03	0.81	7.92	0.74

390 4.2 Determination of marginal distribution and Copula function

391 In the CBMA application for different horizons ($t+1 \sim t+4$), it needs to identify the
 392 best CDFs for fitting the observations (y_t, \dots, y_{t+4}) and i th model forecasts
 393 ($M_{i,t+1}, \dots, M_{i,t+4}$). It seems reasonable to consider that the observations (y_t, \dots, y_{t+4})
 394 follow the same marginal CDF of the variable (y_t) and therefore only the cumulative
 395 distribution functions of the observation (y_t) and model forecasts ($M_{i,t+1}, \dots, M_{i,t+4}$)

396 need to be fitted (Koutsyiannis and Montanari, 2015; Liu et al., 2018).



(b) S-ANFIS forecasts (M_t) (c) M-SVM forecasts (M_t) (d) S-NARX forecasts (M_t) (e) M-LSTM forecasts (M_t)

Figure. 4 Statistic indicator (D) values for verifying the null hypothesis at the 5% significance level in the training stages at the Traffic Station A1. The critical value of statistic indicator (D) = 0.047. The large values (≥ 0.047) of statistic indicator (D) indicate that the null hypothesis for candidate distribution would be rejected at the 5% significance level and the small values (< 0.047) of statistic indicator (D) indicate that the null hypothesis for candidate distribution cannot be rejected at the 5% significance level.

1 405 Take traffic Station A1 for example, Figure 4 summarized the K-S statistic
2
3 406 indicator values (D), which was used to verify the null hypothesis at the 5%
4
5
6 407 significance level in the training stages. The null hypothesis was defined as the
7
8
9 408 marginal distribution follows one candidate distribution, against the alternative that it
10
11
12 409 did not follow such a candidate distribution. The results suggested that the null
13
14
15 410 hypothesis for all four candidate distributions could not be rejected at the 5%
16
17
18 411 significance level (critical value = 0.047), other than Gaussian and Pearson type III
19
20
21 412 distributions. That is to say, both observations and model forecasts have non-Gaussian
22
23
24 413 and Pearson type III properties. The Gumbel distribution provided minimal D values
25
26
27 414 for all observations while the Log-Weibull distribution provided minimal D values for
28
29
30 415 all model forecasts. In other words, the Gumbel distribution and the Log-Weibull
31
32
33 416 distribution would be considered as the best fitted distributions for observations (y_t)
34
35
36 417 and model forecasts ($M_{i,t+1}, \dots, M_{i,t+4}$) respectively.

36 418 When the best marginal distribution was determined, a Copula function should be
37
38
39 419 selected to model the joint distribution between model forecasts ($M_{i,t}$) and
40
41
42 420 observations (y_t). Take the Traffic Station A1 for example, Table 3 presented the
43
44
45 421 estimated parameters of the three candidate copula functions and the values of statistic
46
47
48 422 indicator (D) in the training stages. The null hypothesis was defined as the joint
49
50
51 423 distribution follows one candidate Copula function, against the alternative that it did
52
53
54 424 not follow such a candidate Copula function. The results revealed that the null
55
56
57 425 hypothesis for two candidate distributions could not be rejected at the 5% significance
58
59
60 426 level (critical value = 0.047), other than Clayton Copula function. The smallest K-S

427 statistic indicator (D) was produced by the Gumbel-Hougaard Copula function.

428 Consequently, the Gumbel-Hougaard Copula function could be considered as the best

429 fitted joint distribution between observations (y_t) and model forecasts ($M_{i,t}$).

430 **Table 3** Estimated parameters of the candidate copula functions and the values of
 431 statistic indicator (D) in the training stages at the Traffic Station A1

Model	Variables	Gumbel-Hougaard		Frank		Clayton	
		θ	D	θ	D	θ	D
S-ANFIS	(y_t, M_{t+1})	9.3	*0.017	21.4	0.023	16.6	0.092
	(y_t, M_{t+2})	9.0	0.022	20.7	0.027	16.0	0.105
	(y_t, M_{t+3})	8.6	0.029	19.8	0.034	15.2	0.111
	(y_t, M_{t+4})	8.1	0.036	18.6	0.040	14.2	0.124
M-SVM	(y_t, M_{t+1})	9.6	0.015	22.0	0.020	17.2	0.094
	(y_t, M_{t+2})	9.1	0.021	20.9	0.025	16.2	0.102
	(y_t, M_{t+3})	8.8	0.027	20.2	0.031	15.6	0.114
	(y_t, M_{t+4})	8.3	0.034	19.0	0.038	14.6	0.128
S-NARX	(y_t, M_{t+1})	10.3	0.012	22.3	0.016	18.6	0.085
	(y_t, M_{t+2})	9.8	0.016	21.2	0.020	17.6	0.094
	(y_t, M_{t+3})	9.3	0.021	20.1	0.025	16.6	0.109
	(y_t, M_{t+4})	8.9	0.030	19.3	0.032	15.8	0.120
M-LSTM	(y_t, M_{t+1})	10.2	0.014	22.5	0.017	18.4	0.089
	(y_t, M_{t+2})	9.8	0.017	21.6	0.021	17.6	0.097
	(y_t, M_{t+3})	9.4	0.020	20.7	0.027	16.8	0.105
	(y_t, M_{t+4})	9.0	0.028	19.9	0.034	16.0	0.117

432 *A number in bold denotes the smallest value of statistic indicator (D) in its category. The values of
 433 y_t are the observed $PM_{2.5}$ concentrations of Traffic Station A1 at the current time t . The values of M_{t+1} ,
 434 M_{t+2} , M_{t+3} , M_{t+4} are the ANN models forecasts of $PM_{2.5}$ concentrations of Traffic Station A1 at the
 435 horizons from $t+1$ to $t+4$. The critical value of statistic indicator (D) = 0.047. The large values (\geq
 436 0.047) of statistic indicator (D) indicate that the null hypothesis for candidate distribution would
 437 be rejected at the 5% significance level and the small values (< 0.047) of statistic indicator (D)
 438 indicate that the null hypothesis for candidate distribution cannot be rejected at the 5%
 439 significance level.

441 4.3 Ensemble $PM_{2.5}$ forecasts

442 Moreover, QQ plots were employed to assess the reliability of ensemble $PM_{2.5}$
 443 forecasts. Figure 5 presented the predictive QQ plots used for ensemble $PM_{2.5}$
 444 forecasting (e.g. traffic Station A1, general Station A3 & park Station A5) from
 445 horizons $t+1$ up to $t+4$ in the testing stages, respectively.

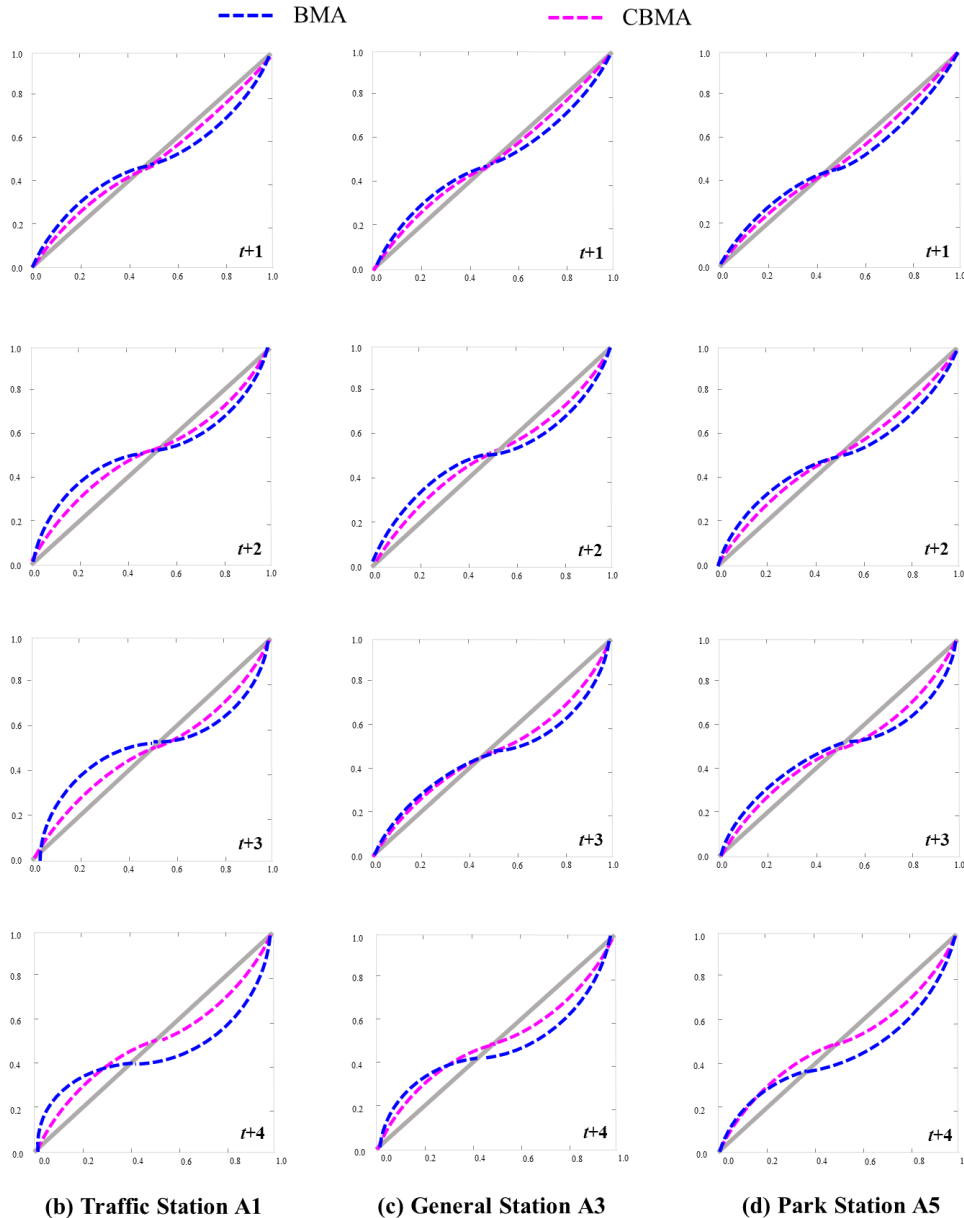
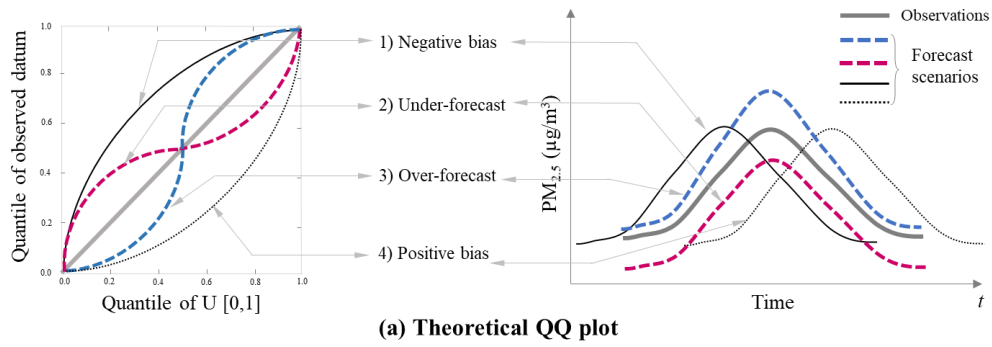
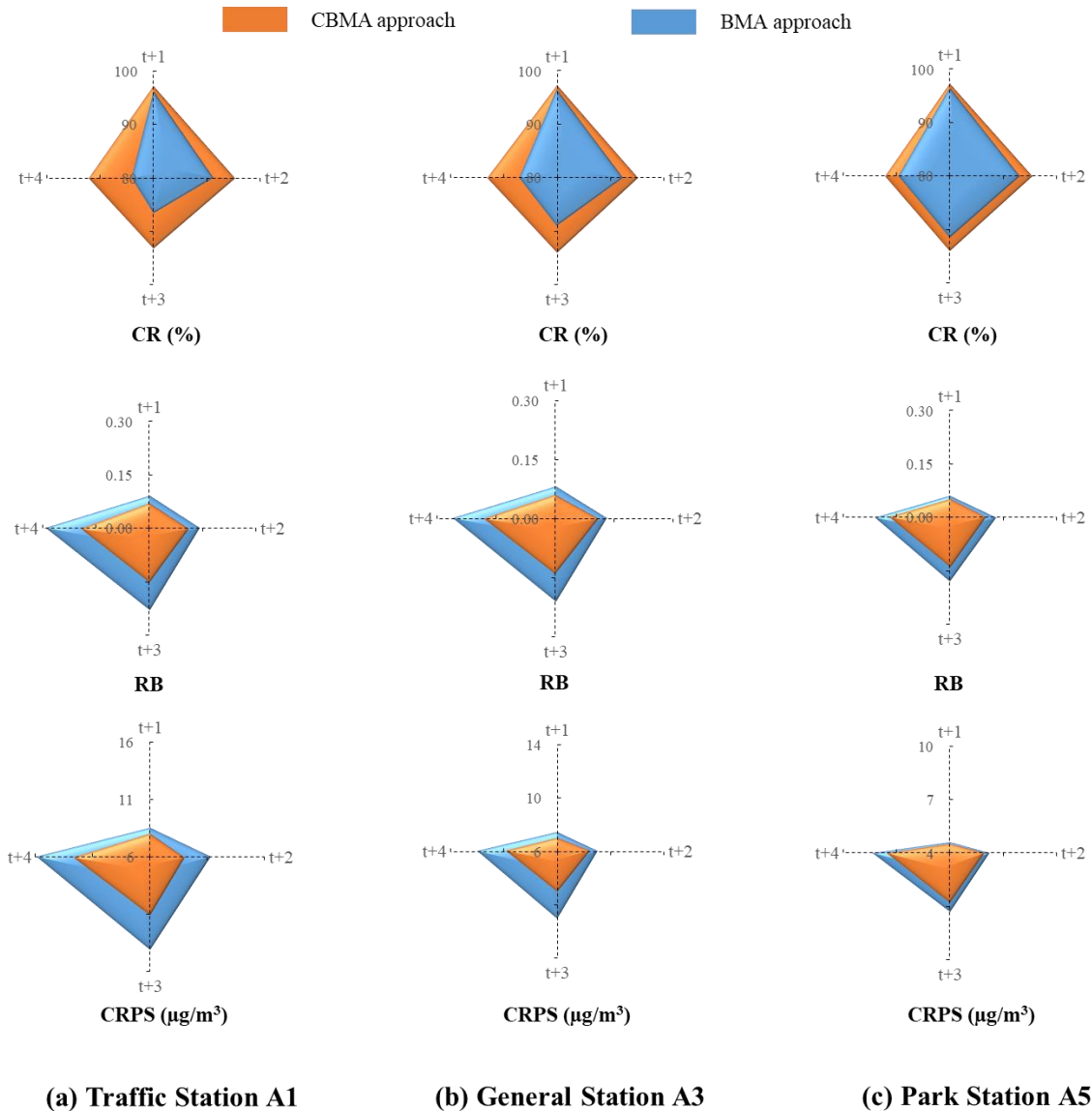


Figure. 5 Predictive Quantile-Quantile (QQ) plots for ensemble $PM_{2.5}$ forecasts from horizons $t+1$ up to $t+4$ in the testing stages at the traffic Station A1, general Station A3 and park Station A5 respectively. The quantile of observed datum is the probability value corresponding to the observed datum while the quantile of $U[0, 1]$ is the probability value corresponding to the forecasted datum.

1 452 According to Figures 5(b) and 5(c), it was easy to find that the QQ plot generated by
2
3 453 the CBMA approach was closer to the 1:1 line, in comparison to that of the BMA one.
4
5
6 454 That is to say, the CBMA approach produced higher reliability and smaller bias than
7
8
9 455 the BMA one. The results pointed out that the CBMA approach could effectively
10
11
12 456 quantify predictive uncertainty owing to its better agreement between the predictive
13
14
15 457 distribution and the observations. This finding demonstrated that the CBMA approach
16
17
18 458 performed significantly better from the perspective of reliability.

19
20 459 For the ensemble PM_{2.5} forecasts (e.g. Traffic Station A1, General Station A3 &
21
22
23 460 Park Station A5) at horizons from t+1 up to t+4, the values of CR, RB and CRPS
24
25
26 461 scores were listed in Figure 6. For the Traffic Station A1 and the General Station A3,
27
28
29 462 the CBMA approach produced better performance in all horizons whereas the BMA
30
31
32 463 performed well only at horizons up to t+2 (e.g. CR was higher than 90%, RB was
33
34
35 464 lower than 0.15 and CRPS was lower than 12 µg/m³ at the Station A1). For the Park
36
37
38 465 Station A5, the BMA approach performed as well as the CBMA approach in all
39
40
41 466 horizons. Take the Traffic Station A1 for example, the BMA approach produced small
42
43
44 467 CR values, whereas the CBMA approach produced small RB and CRPS values. For
45
46
47 468 horizon t+4, the CBMA approach could improve the CR value by 9.58 % as well as
48
49
50 470 BMA one. That is to say, the CBMA approach not only could largely increase
51
52
53 471 ensemble forecast accuracy at the goodness of the prediction bounds (in terms of CR
54
55
56 472 and CRPS values) but also could decrease the impact of PM_{2.5} concentration
57
58
59 473 magnitude on the band-width of the prediction bounds (in terms of RB values)

474 simultaneously.



475
476 **Figure. 6** CBMA and BMA performance of ensemble $PM_{2.5}$ forecasts in the testing
477 stage at the traffic Station A1, general Station A3 and park Station A5. All of indicator
478 values are computed for the 90% prediction intervals.

479
480 The results demonstrated that the CBMA approach had higher reliability and
481 generalizability for ensemble $PM_{2.5}$ forecasting, in comparison to the BMA one. The
482 reason for causing the forecast accuracy of the CBMA approach superior to the BMA
483 one consisted of: the Copula functions in CBMA approach were able to eliminate
484 forecast bias and characterize the correlations between observed values and forecast

1 485 values so that the forecast errors and biases could be reduced significantly. In
2
3
4 486 consequence, the simple bias correction with linear regression method would not need
5
6 487 in the application of Copula functions in the CBMA approach, as compared to the
7
8
9 488 BMA one.

10
11 489 The weights created by CBMA and BMA approaches in the training stage were
12
13
14 490 presented in Figure 7. Each data point suggested the weights (CBMA & BMA) for
15
16
17 491 various models and different horizons ($t+1 \sim t+4$); there were 16 data points (4
18
19
20 492 (models) \times 4 (horizons) = 16) in each subplot. Except in the Park Station A5
21
22
23 493 (correlation coefficient $R = 0.65$), the correlation of weights ($R = -0.11 \sim 0.37$) was
24
25
26 494 very small, which could clearly demonstrate the different performance of CBMA and
27
28
29 495 BMA. It was noted from Eqs. (5) and (8) that the weight of each model in the BMA
30
31 496 (or CBMA) approach was expressed as a function of the latent variable $v_i^t(j)$ (or
32
33
34 497 $z_i^t(j)$) and the posterior probability of training data was employed to compute it.
35
36
37 498 Hence, the CBMA approach was not only restricted to the model diversity and the
38
39
40 499 shape of posterior distributions, but it also had an effect on the weights assigned to
41
42 500 each forecast model and the performance of EM algorithm.
43
44
45
46
47
48
49
50
51
52
53
54
55
56
57
58
59
60
61
62
63
64
65

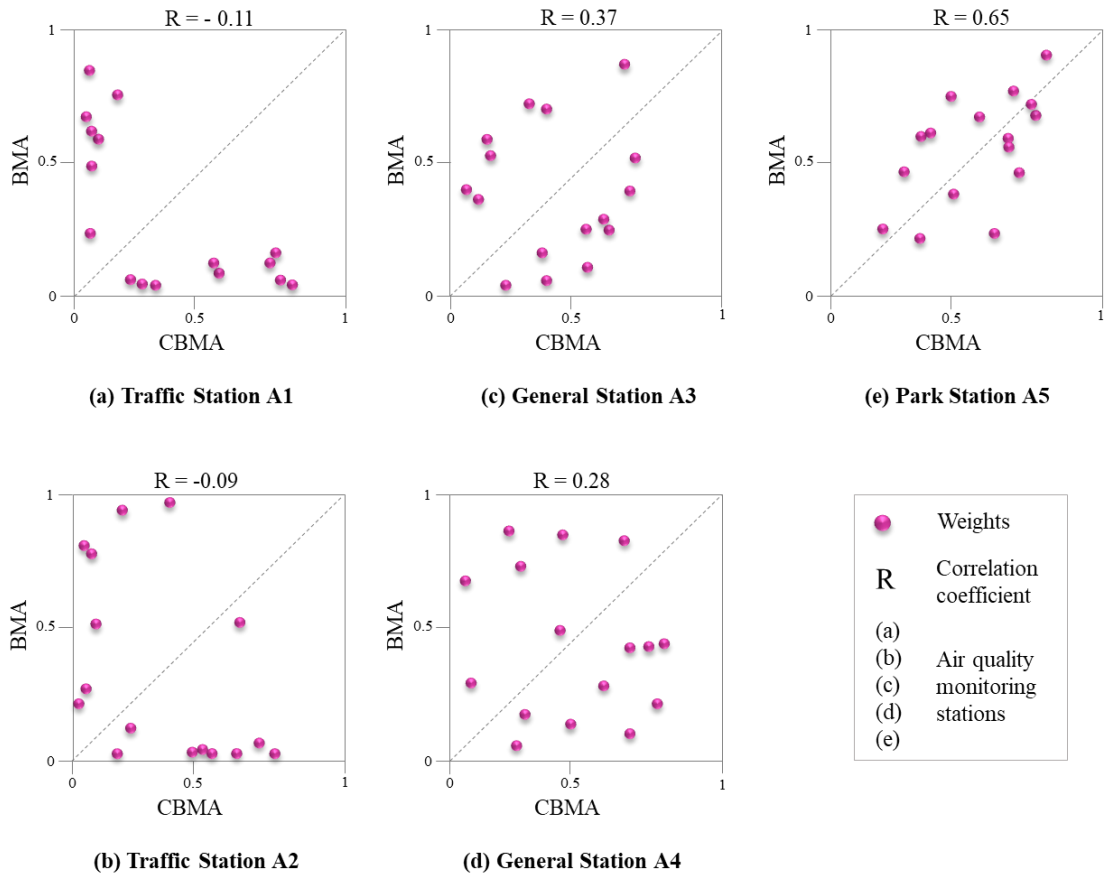
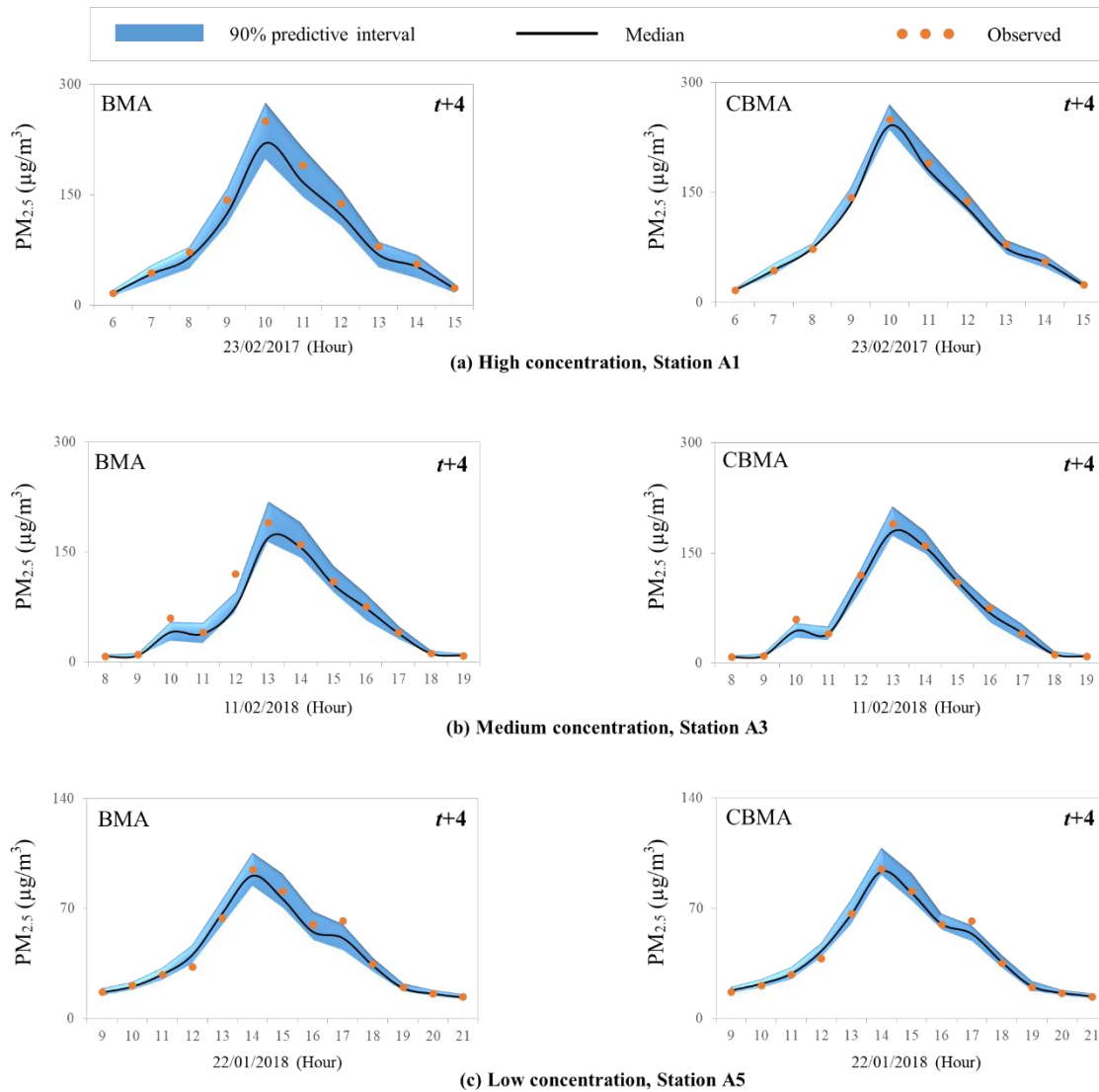


Figure. 7 Comparing the weights of four ANN models for the horizons ($t+1$ to $t+4$) in the training stage after the application of CBMA and BMA for each station.

To clearly differentiate the capabilities of the BMA and the CBMA approaches, three $PM_{2.5}$ events with maximal $PM_{2.5}$ concentrations reaching $80 \mu\text{g}/\text{m}^3$ (low), $160 \mu\text{g}/\text{m}^3$ (medium) and $250 \mu\text{g}/\text{m}^3$ (high), respectively, were applied for testing both approaches by evaluating whether the observed $PM_{2.5}$ concentrations fell within the 90% prediction interval at horizon $t+4$ in the testing stages, as shown in Figure 8. It revealed that: (1) most of the observed $PM_{2.5}$ concentrations fell within the 90% prediction intervals generated by both approaches, (2) the CBMA approach provided better results in terms of predictive distribution, and (3) the CBMA approach was magically superior to that of the BMA one. From air pollutant mechanisms' perspective, primary emission's impact related to meteorological circumstances (i.e.

1 514 park Station A5) on the BMA and CBMA approaches was not significant, while
2
3 515 secondary emission's impact related to meteorological circumstances (i.e. traffic
4
5
6 516 Station A1 and general Station A3) on the BMA and CBMA approaches made a
7
8
9 517 significant difference. For Taipei City, a fast urban growth city, regional air quality
10
11
12 518 exchanges with traffic burdens, commercial trading and intensive human activities
13
14 519 frequently. A high PM_{2.5} event driven by secondary processes was closely related with
15
16
17 520 regional transportation of aged secondary aerosol or secondary transformation of
18
19
20 521 gaseous pollutants, whereas a medium-low PM_{2.5} event driven by the primary or
21
22
23 522 natural process was closely related with local weather conditions and primary
24
25
26 523 emissions. Both CBMA and BMA approaches produced a better performance at the
27
28
29 524 traffic station (A1) and general station (A3) than at the park station (A5). In other
30
31 525 words, the CBMA approach not only greatly improved the ensemble forecast accuracy
32
33
34 526 of PM_{2.5} concentration at traffic station and general station, but also performed as well
35
36
37 527 as the BMA approach at the park station.
38
39
40
41
42
43
44
45
46
47
48
49
50
51
52
53
54
55
56
57
58
59
60
61
62
63
64
65



528
 529 **Figure. 8** BMA and CBMA ensemble $PM_{2.5}$ forecasts for air quality monitoring
 530 Stations A1, A3 and A5 at horizon $t+4$ respectively. Three $PM_{2.5}$ events with maximal
 531 $PM_{2.5}$ concentrations exceeding (a) $250 \mu\text{g}/\text{m}^3$ (high concentration, Station A1), (b)
 532 $160 \mu\text{g}/\text{m}^3$ (medium concentration, Station A3) and (c) $80 \mu\text{g}/\text{m}^3$ (low concentration,
 533 Station A5) were selected for testing the constructed models, respectively.

534 In brief, from the standpoint of model performance, RMSE and G_{bench} were
 535 employed to evaluate the accuracy of deterministic $PM_{2.5}$ forecasts while QQ plot, CR,
 536 RB and CRPS indicators were employed to evaluate the reliability (QQ plot) and
 537 sharpness (CR, RB and CRPS) of ensemble $PM_{2.5}$ forecasts. The CBMA approach not
 538 only could produce more stable and accurate ensemble forecasts but also could reduce
 539 the predictive distributions encountered in multi-step-ahead $PM_{2.5}$ forecasts to small

1 540 ranges, by means of removing the requirements of data transformation and bias
2
3 541 correction procedures, in comparison to the BMA approach. In light of
4
5
6 542 methodological transferability, future research would extend the CBMA methodology
7
8
9 543 on ensemble forecasting or comparison analysis studies between data-driven models
10
11 544 and physically-based models (e.g. Weather Research and Forecasting Models).
12
13

14 545

17 546 **5. Conclusions**

20 547 This study explored a CBMA approach for modeling ensemble $PM_{2.5}$ forecasts of 5
21
22 548 air quality monitoring stations located in the Taipei City of Taiwan and the standard
23
24
25 549 BMA one was selected as a benchmark. First, four ANN models with different
26
27
28 550 complexities were used for $PM_{2.5}$ forecasts of each air quality monitoring station. And
29
30
31 551 then, the CBMA approach and the BMA approach were compared in ensemble $PM_{2.5}$
32
33
34 552 forecasting.

36 553 The results demonstrated that the CBMA approach displayed better ensemble
37
38
39 554 forecast skill in comparison to the BMA one. First, in terms of CR, RB and CRPS
40
41
42 555 indicator values, forecast accuracy and reliability increased significantly after
43
44
45 556 applying the CBMA approach in all air quality monitoring stations. For horizons $t+1$
46
47
48 557 up to $t+4$, the CBMA approach would increase the values of CR indicator by 3.12% -
49
50
51 558 9.58% as well as decrease the values of RB indicator by 8.63% - 34.48% and the
52
53
54 559 values of CRPS indicator by 7.62% - 32.89%, as compared to the BMA one. Second,
55
56
57 560 results of QQ plots indicated that less bias, and more reliable forecast results when the
58
59
60 561 CBMA approach was employed as a post-processing technique for multiple
61
62
63
64
65

1 562 deterministic models. In comparison to BMA, the CBMA approach could create a
2
3 563 more precise predictive distribution with small uncertainty. The CBMA approach
4
5
6 564 produced much better forecasts on the air quality concentrations at longer forecast
7
8
9 565 horizons and significantly alleviated underpredicting phenomena. The reason that the
10
11 566 CBMA approach succeeded in attaining favorable ensemble forecasts would be owing
12
13
14 567 to the core strategy: the use of the Copula function could capture the dependence
15
16
17 568 structure between variables, which avoided their transformation in the Gaussian space
18
19
20 569 as it was done in the BMA approach.
21

22 570 Therefore, the CBMA approach in place of the BMA one would be in the interest
23
24
25 571 of reducing the predictive uncertainty of real-time $PM_{2.5}$ forecasting. In the
26
27
28 572 application of the CBMA approach, the key point was to detect and select a suitable
29
30
31 573 marginal PDF for each observation and model forecast, and then a Copula function
32
33
34 574 was constructed for modelling a joint PDF between observation and model forecast.
35
36
37 575 Finally, it was worth noting that the computational time (less than 2 minutes) of the
38
39
40 576 proposed approach was extremely short and therefore it could be applied with success
41
42
43 577 to real-time air quality forecasting.
44

45 578 From the perspective of regional $PM_{2.5}$ characteristics, Taipei City acts as
46
47
48 579 Taiwan's political, economic and cultural center, while its air quality concentrations
49
50
51 580 are attributed to high traffic influences, high human activities and commercial trading
52
53
54 581 influences in comparison to these in other cities of Taiwan. The proposed
55
56
57 582 methodology could be effectively employed not only to model the heterogeneities in
58
59
60 583 different air pollutant-generating mechanisms (e.g., primary and secondary
61
62
63
64
65

1 584 mechanisms, and natural situations) and different seasons, but also to provide reliable
2
3 585 and accurate probabilistic regional PM_{2.5} forecasts in the interest of Taiwan's social
4
5
6 586 and industrial development.
7

8
9 587

10 11 588 **Appendix A**

12 13 589 *General implementation procedure of BMA approach*

14
15
16
17 590 **Step 1:** Implement bias-correction. One requirement of BMA application is that the
18
19
20 591 model forecasts $M_{i,t}$ should be bias-corrected due to the non-bias assumption. A
21
22
23 592 bias-correction with linear regression method suggested by Raftery et al. (2005) was
24
25
26 593 adopted prior to BMA execution and the original model forecast results ($M_{i,t}$) ought
27
28 594 to be substituted by the bias-corrected forecast variables ($f_{i,t}$).

$$29
30
31 595 \quad \quad \quad f_{i,t} = a_i + b_i M_{i,t} \quad (1)$$

32
33
34 596 where $f_{i,t}$ and $M_{i,t}$ are the i th bias-corrected value and original model forecast
35
36
37 597 respectively. a_i and b_i are the linear regression coefficients of i th model forecast.

38
39 598 **Step 2:** Transform data space. Another requirement of BMA application is that the
40
41
42 599 bias-corrected values ($f_{i,t}$) should be converted to special datasets with a Gaussian
43
44
45 600 space. Box-Cox transformation proposed by Box and Cox (1964) was used to conduct
46
47
48 601 data transformation and was described as below.

$$49
50
51 602 \quad \quad \quad f_{i,t}^\lambda = \begin{cases} \frac{f_{i,t}^\lambda - 1}{\lambda} & \lambda \neq 0 \\ \ln(f_{i,t}) & \lambda = 0 \end{cases} \quad (2)$$

52
53
54 603 where $f_{i,t}^\lambda$ and λ are the bias-corrected value of i th model at the t time and Box-Cox
55
56
57 604 coefficient respectively. In this study, the artificial covariate method (Dag et al., 2013)
58
59
60 605 was employed to determine the optimal value of Box-Cox coefficient while the K-S

1 606 test statistic (Lilliefors, 1967) was employed to prove the Gaussianity of the
2
3 607 transformed data. After implementation of the data transformation, the posterior
4
5
6 608 distribution $p(y_t|f_{i,t}^\lambda, Y)$ would follow a Gaussian distribution
7
8
9 609 $p(y_t|f_{i,t}^\lambda, Y) \sim g(y_t|f_{i,t}^\lambda, \delta_i^2)$.

10
11 610 **Step 3:** Estimate parameters. A log-likelihood function was adopted to estimate the
12
13
14 611 parameters of weight (ω_i) and variance (δ_i^2) and was formulated as follows.

$$17 \quad 612 \quad l_\varphi = \log(\sum_{i=1}^k \omega_i p(y_t|f_{i,t}^\lambda, Y)) \quad (3)$$

18
19
20 613 where $\boldsymbol{\varphi}$ is the vector of parameters $\{\omega_i, \delta_i^2, i = 1, 2, \dots, k\}$.

21
22
23 614 The Expectation-Maximization (EM) suggested by Raftery et al. (2005) was
24
25
26 615 utilized to search the optimal parameters of weight (ω_i) and variance (δ_i^2) when a
27
28
29 616 termination criterion (early stopping or the maximal iteration) was achieved. As the
30
31
32 617 EM algorithm proceeds, the parameters of weight (ω_i) and variance (δ_i^2) were
33
34 618 updated as follows.

$$36 \quad 619 \quad \omega_i(j) = \frac{1}{T} \sum_{t=1}^T v_i^t(j) \quad (4a)$$

$$40 \quad 620 \quad \delta_i^2(j) = \frac{\sum_{t=1}^T v_i^t(j) (y_t - f_{i,t}^\lambda)^2}{\sum_{t=1}^T v_i^t(j)} \quad (4b)$$

$$44 \quad 621 \quad v_i^t(j) = \frac{\omega_{i(j-1)} \cdot g(y_t|f_{i,t}^\lambda, \delta_{i(j-1)}^2)}{\sum_{i=1}^k \omega_{i(j-1)} \cdot g(y_t|f_{i,t}^\lambda, \delta_{i(j-1)}^2)} \quad (4c)$$

$$48 \quad 622 \quad l_\varphi(j) = \log\left(\sum_{i=1}^k \omega_i(j) \sum_{t=1}^T g(y_t|f_{i,t}^\lambda, \delta_i^2(j))\right) \quad (4d)$$

50 623 where T is the number of the training datasets and $v_i^t(j)$ is the latent variable for the
51
52
53 624 i th model at the t time in the j th iteration.

54
55
56 625 **Step 4:** Create BMA ensemble forecasts. After the parameters of weight (ω_i) and
57
58
59 626 variance (δ_i^2) were estimated, we used the Monte Carlo simulation method to generate

627 BMA ensemble forecasts (Raftery, 2005; Zhou et al., 2016). The procedure was

628 described as follows.

629 a) Generate an integer value of i in $[1, 2, \dots, k]$ by using the corresponding

630 probabilities $[\omega_1, \omega_2, \dots, \omega_k]$. Set the initial cumulative weight $\omega_0^* = 0$ and

631 calculate cumulative weight $\omega_i^* = \omega_{i-1}^* + \omega_i$ for $i = 1, 2, \dots, k$. Create a random

632 variable u between 0 and 1. If $\omega_{i-1}^* \leq u \leq \omega_i^*$, it indicates that the i th model forecast

633 would be selected and used in the next step.

634 b) Generate a realization of the observation y_t using the PDF $g(y_t | f_{i,t}^\lambda, \delta_i^2)$.

635 c) Repeat the above two steps (a) & b)) for K times. K is the number of Monte Carlo

636 simulation and set as 1000 in this study. At last, data conversion is needed to convert

637 the ensemble forecasts from a Gaussian space to their original space. Furthermore, 90 %

638 confidence intervals between the 5 % and 95 % quantities were employed to reveal

639 the uncertainty of BMA ensemble forecasts.

640

641 **Appendix B**

642 *General implementation procedure of CBMA approach*

643 **Step 1:** Configure the marginal distributions of the forecast variable of each model

644 $(M_{i,t})$ and realization of observation (y_t) respectively. Let $U_M = P_M(M_{i,t})$ and

645 $U_y = P_y(y_t)$ are the Cumulative Distribution Functions (CDFs) of the forecast

646 variable of each model $(M_{i,t})$ and realization of observation (y_t) respectively. It would

647 specify and determine the marginal distribution $P_M(M_{i,t})$ of the forecast variable of

648 each model $(M_{i,t})$ and the marginal distribution $P_y(y_t)$ of the realization of

649 observation (y_t) to construct posterior probability in the next step. Seven different
650 probability distributions, including Gaussian, Gamma, Gumbel, Pearson type III,
651 Generalized Extreme Value (GEV) and Log-Weibull were tried in this study and
652 summarized in Table 1.

653 **Table 1** Candidate univariate distributions adopted for fitting the marginal
654 distributions

Distribution	Probability distribution function (pdf)	Range	Parameters
Gaussian	$f(x) = \frac{1}{\sqrt{2\pi}\sigma} \exp\left[-\frac{(x-\mu)^2}{2\sigma^2}\right]$	$-\infty < x < +\infty$	μ σ
Gamma	$f(x) = \frac{\beta^\alpha}{\Gamma(\alpha)} x^{\alpha-1} \exp(-\beta x)$	$x > 0$	α β
Gumbel	$f(x) = \alpha \exp[-\alpha(x-\mu) - e^{-\alpha(x-\mu)}]$	$-\infty < x < +\infty$	α μ
GEV	$f(x) = \frac{1}{\sigma} \left[1 + \gamma \left(\frac{x-\mu}{\sigma}\right)\right]^{(-1/\gamma)-1} \cdot \exp\left\{-\left[1 + \gamma \left(\frac{x-\mu}{\sigma}\right)\right]^{-1/\gamma}\right\}$	$-\infty < x < +\infty$	μ σ γ
Person type III	$f(x) = \frac{\beta^\alpha}{\Gamma(\alpha)} (x-\mu)^{\alpha-1} \exp[-\beta(x-\mu)]$	$x > \mu$	α β μ
Log-Weibull	$f(x) = \frac{1}{\alpha(x-\mu+1)} \left[\frac{\ln(x-\mu+1)}{\alpha}\right]^{\beta-1} \cdot \exp\left\{-\left[\frac{\ln(x-\mu+1)}{\alpha}\right]^\beta\right\}$	$x > \mu$	α β μ

655 Owing to the wide practicality of the L-moments method (Hosking, 1990; Zhou
656 et al., 2014) and the K-S statistic test method (Lilliefors, 1967; Razali and Wah, 2011),
657 these two methods were used to estimate the distribution parameters and find the best
658 marginal distribution respectively. The 5% significance level was applied to deciding
659 whether a fitted distribution was acceptable or not, and then the probability
660 distribution that possessed the minimum K-S test statistic indicator D (i.e. the
661 maximum difference between the values of the empirical and the expected cumulative
662 distributions) value was recommended as the best fitted distribution.

663 **Step 2:** Apply Copula function to constructing the posterior probability of forecast
664 variable of each model $p(y_t | M_{i,t}, Y)$. Various family members of Copula functions

665 have been introduced by Nelsen (2006). The Archimedean Copula functions have
 666 impressive practicality in hydrologic and meteorological research domains because it
 667 is easy to construct (e.g. Chen and Guo, 2019; Zhang and Singh, 2019).

668 **Table 2** Candidate bivariate Archimedean copula functions

Copula function	Joint distribution function	Parameter
Gumbel-Hougaard	$C(u_1, u_2 \theta) = \exp\{-[(-\ln u_1)^\theta + (-\ln u_2)^\theta]^{1/\theta}\}$	$*\tau = 1 - \frac{1}{\theta}$ $\theta \geq 1$
Frank	$C(u_1, u_2 \theta) = -\frac{1}{\theta} \ln \left[1 + \frac{[\exp(-\theta u_1) - 1][\exp(-\theta u_2) - 1]}{\exp(-\theta) - 1} \right]$	$\tau = 1 + \frac{4}{\theta} \left[\frac{1}{\theta} \int_0^\theta \frac{t}{\exp(t)} dt - 1 \right]$ $-\infty < \theta < +\infty$
Clayton	$C(u_1, u_2 \theta) = (u_1^{-\theta} + u_2^{-\theta} - 1)^{-1/\theta}$	$\tau = \frac{\theta}{2 + \theta}$ $\theta > 0$

669 * τ is the Kendall's coefficient.

670 In this study, three Copula functions were tested, including Gumbel-Hougaard,
 671 Clayton and Frank from Archimedean Copula functions (Table 2). Then, the Kendall's
 672 coefficient and the K-S statistic test method were employed to estimate the parameter
 673 of Copula functions and choose the best Copula function. The copula function
 674 possessing the smallest K-S statistic indicator (D) at the 5% significance level would
 675 be selected as the most suitable one.

676 **Step 3:** Apply EM algorithm to estimating weight parameter (ω_i) of each model. After
 677 the posterior distribution is constructed, its weight parameter was estimated by using
 678 the EM algorithm by means of a few adjustments in the Eq. (4) of Appendix A.

$$679 \quad \omega_i(j) = \frac{1}{T} \sum_{t=1}^T z_i^t(j) \quad (5a)$$

$$680 \quad z_i^t(j) = \frac{\omega_i(j-1) \cdot p(u_{y_t} | u_{M_{i,t}})}{\sum_{i=1}^k \omega_i(j-1) \cdot p(u_{y_t} | u_{M_{i,t}})} = \frac{\omega_i(j-1) \cdot c_{\theta_i}(u_{M_{i,t}}, u_{y_t}) \cdot p_y(u_{y_t})}{\sum_{i=1}^k \omega_i(j-1) \cdot c_{\theta_i}(u_{M_{i,t}}, u_{y_t}) \cdot p_y(u_{y_t})} \quad (5b)$$

$$681 \quad l_\varphi(j) = \log \left(\sum_{i=1}^k \omega_i(j) \sum_{t=1}^T c_{\theta_i}(u_{M_{i,t}}, u_{y_t}) \cdot p_y(u_{y_t}) \right) \quad (5c)$$

1 682 where $z_i^t(j)$ is the latent variable for the i th model at the t time in the j th iteration
2
3 683 based on the Copula conditional probability. As seen, the estimation of variance
4
5
6 684 parameter (δ_i^2) has not occurred in Eq. (5). Furthermore, the posterior probability
7
8
9 685 $p(u_{y_t}|u_{M_{i,t}})$ is calculated only one time in Eq. (5) and that remains the same for all
10
11 686 the iterations. While the posterior probability $g(y_t|f_{i,t}^\lambda, \delta_i^2(j-1))$ in the BMA (Eq.
12
13 687 (4) in Appendix A) should be computed and updated when the variance parameter (δ_i^2)
14
15 688 changes.

16
17
18
19 689 **Step 4:** Apply the Monte Carlo simulation method for producing the realization of
20
21 690 observation (y_t). a) Generate an integer value of i in $[1, 2, \dots, k]$ by using the
22
23 691 corresponding probabilities $[\omega_1, \omega_2, \dots, \omega_k]$. Set the initial cumulative weight
24
25 692 $\omega_0^* = 0$ and calculate cumulative weight $\omega_i^* = \omega_{i-1}^* + \omega_i$ for $i = 1, 2, \dots, k$. Create
26
27 693 a random variable u between 0 and 1. If $\omega_{i-1}^* \leq u \leq \omega_i^*$, it indicates that the i th
28
29 694 model forecast would be selected and used in the next step. b) Generate a realization
30
31 695 of observation y_t using the conditional PDF $c_{\theta_i}(u_{M_{i,t}}, u_{y_t}) \cdot p_y(u_{y_t})$. c) Repeat the
32
33 696 above two steps (a) & b)) for K times. K is the number of Monte Carlo simulation and
34
35 697 set as 1000 in this study. Similarly, 90 % confidence intervals were employed to
36
37 698 reveal the uncertainty of CBMA ensemble forecasts.

38 39 40 41 42 43 44 45 46 47 48 49 700 **Acknowledgments**

50
51
52
53 701 This work was supported by the Ministry of Science and Technology, Taiwan (MOST
54
55 702 106-3114-M-002-001-A, 108-2119-M-002-017-A, 106-2811-B-002-087-), the
56
57
58 703 Research Council of Norway (FRINATEK Project 274310) and the National Key
59
60
61
62
63
64
65

1 704 Research and Development Program of China (2018YFC0407904). The datasets
2
3 705 provided by the Environmental Protection Administration, Taiwan, are acknowledged.
4
5
6 706 The authors would like to thank the Editors and anonymous Reviewers for their
7
8
9 707 constructive comments that greatly contributed to improving the manuscript.
10

11 708

14 709 **References**

- 16 710 Akbari Asanjan, A., Yang, T., Hsu, K., Sorooshian, S., Lin, J., & Peng, Q., 2018. Short- term
17 711 precipitation forecast based on the PERSIANN system and LSTM recurrent neural
18 712 networks. *J. Geophys. Res.: Atmos.*, 123(22), 12-543.
- 19 713 Ausati, S., & Amanollahi, J., 2016. Assessing the accuracy of ANFIS, EEMD-GRNN, PCR,
20 714 and MLR models in predicting PM_{2.5}. *Atmos. Environ.*, 142, 465-474.
- 21 715 Aznarte, J. L., 2017. Probabilistic forecasting for extreme NO₂ pollution episodes. *Environ.*
22 716 *Pollut.*, 229, 321-328.
- 23 717 Bai, L., Wang, J., Ma, X., & Lu, H., 2018. Air pollution forecasts: An overview. *International*
24 718 *Int. J. Environ. Res. Public Health*, 15(4), 780.
- 25 719 Berardis, D., & Eleonora, M., 2017. Analysis of major pollutants and physico-chemical
26 720 characteristics of PM_{2.5} at an urban site in Rome. *Sci. Total Environ.*, 617, 1457-1468.
- 27 721 Box, G. E. P., and Cox D. R., 1964, An analysis of transformations, *J. R. Stat. Soc. Ser. B*,
28 722 26(2), 211-252.
- 29 723 Breiman, L., & Friedman, J. H., 1997. Predicting multivariate responses in multiple linear
30 724 regression. *J. R. Stat. Soc.*, 59(1), 3-54.
- 31 725 Buckland, S. T., Burnham, K. P., & Augustin, N. H., 1997. Model selection: an integral part
32 726 of inference. *Biometrics*, 603-618.
- 33 727 Cannon, A. J., 2011. Quantile regression neural networks: Implementation in R and
34 728 application to precipitation downscaling. *Comput. Geosci.*, 37(9), 1277-1284.
- 35 729 Chang, F. J., & Tsai, M. J., 2016. A nonlinear spatio-temporal lumping of radar rainfall for
36 730 modeling multi-step-ahead inflow forecasts by data-driven techniques. *J. Hydrol.*, 535,
37 731 256-269.
- 38 732 Chen L., & Guo S., 2019. Copulas and its application in hydrology and water resources.
39 733 Springer Verlag, Singapore.
- 40 734 Chen, S., Kan, G., Li, J., Liang, K., & Hong, Y., 2018. Investigating China's urban air quality
41 735 using big data, information theory, and machine learning. *Pol. J. Environ. Stud.*, 27(2),
42 736 1-8.
- 43 737 Coelho, M. C., Fontes, T., Bandeira, J. M., Pereira, S. R., Tchepel, O., & Dias, D., et al., 2014.
44 738 Assessment of potential improvements on regional air quality modelling related with
45 739 implementation of a detailed methodology for traffic emission estimation. *Sci. Total*
46 740 *Environ.*, 470 (2), 127-137.

- 1 741 Dag, O., Asar O., & Ilk O., 2013. A methodology to implement Box-Cox transformation
2 742 when no covariate is available, *Commun. Stat. Simul. Comput.*, 43(7), 1740–1759.
- 3 743 Djalalova, I., Delle Monache, L., & Wilczak, J., 2015. PM_{2.5} analog forecast and Kalman
4 744 filter post-processing for the Community Multiscale Air Quality (CMAQ) model. *Atmos.*
5 745 *Environ.*, 108, 76-87.
- 6 746 Dunea, D., Pohoata, A., & Iordache, S., 2015. Using wavelet-feedforward neural networks to
7 747 improve air pollution forecasting in urban environments. *Environmental monitoring and*
8 748 *assessment*, 187(7), 477.
- 9 749 Fanizza, C., De Berardis, B., Ietto, F., Soggiu, M. E., Schirò, R., Inglessis, M., & Incoronato,
10 750 F., 2018. Analysis of major pollutants and physico-chemical characteristics of PM_{2.5} at
11 751 an urban site in Rome. *Sci. Total Environ.*, 616, 1457-1468.
- 12 752 Feng, X., Li, Q., Zhu, Y., Hou, J., Jin, L., & Wang, J., 2015. Artificial neural networks
13 753 forecasting of PM_{2.5} pollution using air mass trajectory based geographic model and
14 754 wavelet transformation. *Atmos. Environ.*, 107, 118-128.
- 15 755 Gao, S., Zhao, P., Pan, B., Li, Y., Zhou, M., Xu, J., & Shi, Z., 2018. A nowcasting model for
16 756 the prediction of typhoon tracks based on a long short term memory neural network.
17 757 *Acta Oceanol. Sin.*, 37(5), 8-12.
- 18 758 Garner, G. G., & Thompson, A. M., 2013. Ensemble statistical post-processing of the national
19 759 air quality forecast capability: Enhancing ozone forecasts in Baltimore, Maryland. *Atmos.*
20 760 *Environ.*, 81, 517-522.
- 21 761 Gneiting T., & Raftery AE., 2007. Strictly Proper Scoring Rules, Prediction, and Estimation. *J.*
22 762 *Am. Stat. Assoc.*, 102(477):359–378.
- 23 763 Gneiting, T., 2008. Probabilistic forecasting. *Journal of the Royal Statistical Society: Series A*
24 764 *(Statistics in Society)*, 171(2), 319-321.
- 25 765 Granger, C. W., & Ramanathan, R., 1984. Improved methods of combining forecasts. *J.*
26 766 *Forecasting*, 3(2), 197-204.
- 27 767 Ghazi, S., & Khadir, M. T., 2009. Recurrent Neural Network for Multi-steps ahead prediction
28 768 of PM₁₀ concentration. *Autom. Syst. Eng.*, 3(2), 13-21.
- 29 769 Gong, B., & Ordieres, M. J., 2016. Prediction of daily maximum ozone threshold exceedances
30 770 by preprocessing and ensemble artificial intelligence techniques: case study of Hong
31 771 Kong. *Environ. Model. Softw.*, 84, 290-303.
- 32 772 Han, X., Chen, N., Yan, J., Liu, J., Liu, M., & Karellas, S., 2019. Thermodynamic analysis
33 773 and life cycle assessment of supercritical pulverized coal-fired power plant integrated
34 774 with No.0 feedwater pre-heater under partial loads. *J. Clean. Prod.*, 233, 1106-1122.
- 35 775 Herr, H. D., & Krzysztofowicz, R., 2015. Ensemble Bayesian forecasting system Part I:
36 776 Theory and algorithms. *J. Hydrol.*, 524, 789-802.
- 37 777 Hoeting, J. A., Madigan, D., Raftery, A. E., & Volinsky, C. T., 1999. Bayesian model
38 778 averaging: a tutorial. *Stat. Sci.*, 382-401.
- 39 779 Hosking, J.R.M., 1990. L-moments: analysis and estimation of distributions using linear
40 780 combinations of order statistics. *J. R. Stat. Soc.*, 52 (1), 105-124.
- 41 781 Huang, Y., Shen, H., Chen, H., Wang, R., Zhang, Y., & Su, S., et al., 2014. Quantification of
42 782 global primary emissions of PM_{2.5}, PM₁₀, and TSP from combustion and industrial
43 783 process sources. *Environ. Sci. Technol.*, 48(23), 13834-13843.

- 1 784 Jang, J. S., 1993. ANFIS: adaptive-network-based fuzzy inference system. *IEEE Trans. Syst.*
2 785 *Man. Cybern.*, 23(3), 665-685.
- 3 786 Lohani, A. K., Goel, N. K., & Bhatia, K. K. S., 2014. Improving real time flood forecasting
4 787 using fuzzy inference system. *J. Hydrol.*, 509, 25-41.
- 5 788 Kaminska, J., 2018. Probabilistic forecasting of nitrogen dioxide concentrations at an urban
6 789 road intersection. *Sustainability*, 10(11), 4213.
- 7 790 Khajehei, S., & Moradkhani, H., 2017. Towards an improved ensemble precipitation forecast:
8 791 A probabilistic post-processing approach. *J. Hydrol.*, 546, 476-489.
- 9 792 Koutsoyiannis, D., & Montanari, A., 2015. Negligent killing of scientific concepts: the
10 793 stationarity case. *Hydrol. Sci. J.*, 60 (7-8), 1174-1183.
- 11 794 Krapu, C., & Borsuk, M., 2019. Probabilistic programming: A review for environmental
12 795 modellers. *Environ. Model. Softw.*, 114, 40-48.
- 13 796 Leontaritis, I. J., & Billings, S. A., 1985. Input-output parametric models for non-linear
14 797 systems. Part I: Deterministic non-linear systems, Part II: stochastic non-linear systems.
15 798 *Int. J. Control*, 41(2): 323-344.
- 16 799 Leslie, L. M., & Holland, G. J., 1991. Predicting regional forecast skill using single and
17 800 ensemble forecast techniques. *Mon. Weather Rev.*, 119(2), 425-435.
- 18 801 Li, H., You, S., Zhang, H., Zheng, W., Lee, W. L., Ye, T., & Zou, L., 2018. Analyzing the
19 802 impact of heating emissions on air quality index based on principal component
20 803 regression. *J. Clean. Prod.*, 171, 1577-1592.
- 21 804 Li, L., Xu, C. Y., & Engeland, K., 2013. Development and comparison in uncertainty
22 805 assessment based Bayesian modularization method in hydrological modeling. *J. Hydrol.*,
23 806 486, 384-394.
- 24 807 Lilliefors, H. W., 1967. On the Kolmogorov-Smirnov test for normality with mean and
25 808 variance unknown, *J. Am. Stat. Assoc.*, 62, 399-402.
- 26 809 Lin, B., & Zhu, J., 2018. Changes in urban air quality during urbanization in China. *J. Clean.*
27 810 *Prod.*, 188, 312-321.
- 28 811 Liu, H., Duan, Z., & Chen, C., 2019. A hybrid framework for forecasting PM_{2.5}
29 812 concentrations using multi-step deterministic and probabilistic strategy. *Air Qual., Atmos.*
30 813 *Health*, 1-11.
- 31 814 Liu, Z., Guo, S., Xiong, L., & Xu, C. Y., 2018. Hydrological uncertainty processor based on a
32 815 copula function. *Hydrol. Sci. J.*, 63(1), 74-86.
- 33 816 Lyu, B., Zhang, Y., & Hu, Y., 2017. Improving PM_{2.5} air quality model forecasts in China
34 817 using a bias-correction framework. *Atmosphere*, 8(8), 147.
- 35 818 Lyu, W., Li, Y., Guan, D., Zhao, H., Zhang, Q., & Liu, Z., 2016. Driving forces of Chinese
36 819 primary air pollution emissions: an index decomposition analysis. *J. Clean. Prod.*, 133,
37 820 136-144.
- 38 821 Maidment, D. R., 1993. *Handbook of hydrology*. New York: McGraw-Hill.
- 39 822 Madadgar, S., and Moradkhani, H., 2014, Improved Bayesian multimodeling: Integration of
40 823 copulas and Bayesian model averaging, *Water Resour. Res.*, 50, 9586-9603.
- 41 824 Monteiro, A., Ribeiro, I., Tchepel, O., Sá, E., Ferreira, J., Carvalho, A., & Schaap, M., 2013.
42 825 Bias correction techniques to improve air quality ensemble predictions: focus on O₃ and
43 826 PM over Portugal. *Environ. Model. Assess.*, 18(5), 533-546.

- 827 Mok, K. M., Miranda, A. I., Yuen, K. V., Hoi, K. I., Monteiro, A., & Ribeiro, I., 2017.
828 Selection of bias correction models for improving the daily PM₁₀ forecasts of
829 WRF-EURAD in Porto, Portugal. *Atmos. Pollut. Res.*, 8(4), 628-639.
- 830 Mok, K. M., Yuen, K. V., Hoi, K. I., Chao, K. M., & Lopes, D., 2018. Predicting
831 ground-level ozone concentrations by adaptive Bayesian model averaging of statistical
832 seasonal models. *Stoc. Environ. Res. Risk. Assess.*, 32(5), 1283-1297.
- 833 Nelsen, R.B., 2006. *An Introduction to Copulas*. Second. New York: Springer.
- 834 Nieto, P. J. G., Lasheras, F. S., García-Gonzalo, E., & Juez, F. J. D. C., 2018. PM₁₀
835 concentration forecasting in the metropolitan area of Oviedo (Northern Spain) using
836 models based on SVM, MLP, VARMA and ARIMA: a case study. *Sci. Total Environ.*,
837 621, 753-761.
- 838 Pannullo, F., Lee, D., Waclawski, E., & Leyland, A. H., 2016. How robust are the estimated
839 effects of air pollution on health? Accounting for model uncertainty using Bayesian
840 model averaging. *Spat. Spatio-Temporal. Epidemiol.*, 18, 53-62.
- 841 Prasad, K., Gorai, A. K., & Goyal, P., 2016. Development of ANFIS models for air quality
842 forecasting and input optimization for reducing the computational cost and time. *Atmos.*
843 *Environ.*, 128, 246-262.
- 844 Pucer, J. F., Pirš, G., & Štrumbelj, E., 2018. A Bayesian approach to forecasting daily
845 air-pollutant levels. *Know. Inf. Syst.*, 57(3), 635-654.
- 846 Raftery, A. E., Gneiting, T., Balabdaoui, F., & Polakowski, M., 2005. Using Bayesian model
847 averaging to calibrate forecast ensembles. *Mon. Weather Rev.*, 133(5), 1155-1174.
- 848 Razali, N. M., & Wah, Y. B., 2011. Power comparisons of Shapiro-Wilk,
849 Kolmogorov-Smirnov, Lilliefors and Anderson-Darling tests. *J. Statis. Model. Anal.*,
850 2(1), 21-33.
- 851 Ryan, W. F., 2016. The air quality forecast rote: Recent changes and future challenges. *J. Air*
852 *Waste Manage. Assoc.*, 66(6), 576-596.
- 853 Shen, C., Laloy, E., Elshorbagy, A., Albert, A., Bales, J., Chang, F. J., et al., 2018. HESS
854 Opinions: Incubating deep-learning-powered hydrologic science advances as a
855 community. *Hydrol. Earth Syst. Sci.*, 22(11), 5639-5656.
- 856 Sun, Y., Du, W., Fu, P., Wang, Q., Li, J., Ge, X., & Zhao, J., 2016. Primary and secondary
857 aerosols in Beijing in winter: sources, variations and processes. *Atmos. Chem. Phys.*,
858 16(13), 8309-8329.
- 859 Taghavifar, H., Taghavifar, H., Mardani, A., Mohebbi, A., Khalilarya, S., & Jafarmadar, S.,
860 2016. Appraisal of artificial neural networks to the emission analysis and prediction of
861 CO₂, soot, and NO_x of n-heptane fueled engine. *J. Clean. Prod.*, 112, 1729-1739.
- 862 Thielen-del Pozo, J., & Bruen, M., 2019. Overview of Forecast Communication and Use of
863 Ensemble Hydrometeorological Forecasts. *Handbook of Hydrometeorological Ensemble*
864 *Forecasting*, 1037-1045.
- 865 Van Fan, Y., Perry, S., Klemeš, J. J., & Lee, C. T., 2018. A review on air emissions
866 assessment: Transportation. *J. Clean. Prod.*, 194, 673-684.
- 867 Voukantsis, D., Karatzas, K., Kukkonen, J., Räsänen, T., Karppinen, A., & Kolehmainen, M.,
868 2011. Intercomparison of air quality data using principal component analysis, and
869 forecasting of PM₁₀ and PM_{2.5} concentrations using artificial neural networks, in
870 Thessaloniki and Helsinki. *Sci. Total Environ.*, 409(7), 1266-1276.

- 1
2
3
4
5
6
7
8
9
10
11
12
13
14
15
16
17
18
19
20
21
22
23
24
25
26
27
28
29
30
31
32
33
34
35
36
37
38
39
40
41
42
43
44
45
46
47
48
49
50
51
52
53
54
55
56
57
58
59
60
61
62
63
64
65
- 871 Weber, S. A., Insaf, T. Z., Hall, E. S., Talbot, T. O., & Huff, A. K., 2016. Assessing the
872 impact of fine particulate matter (PM_{2.5}) on respiratory-cardiovascular chronic diseases
873 in the New York City Metropolitan area using Hierarchical Bayesian Model estimates.
874 *Environ. Res.*, 151, 399-409.
- 875 Wu, J., Zheng, H., Zhe, F., Xie, W., & Song, J., 2018. Study on the relationship between
876 urbanization and fine particulate matter (PM_{2.5}) concentration and its implication in
877 China. *J. Clean. Prod.*, 182, 872-882.
- 878 Xu, S., An, X., Qiao, X., Zhu, L., & Li, L., 2013. Multi-output least-squares support vector
879 regression machines. *Pattern. Recognit. Lett.*, 34(9), 1078-1084.
- 880 Yeganeh, B., Hewson, M. G., Clifford, S., Tavassoli, A., Knibbs, L. D., & Morawska, L.,
881 2018. Estimating the spatiotemporal variation of NO₂ concentration using an adaptive
882 neuro-fuzzy inference system. *Environ. Model. Softw.*, 100, 222-235.
- 883 Yu, H., & Stuart, A. L., 2017. Impacts of compact growth and electric vehicles on future air
884 quality and urban exposures may be mixed. *Sci. Total Environ.*, 576, 148-158.
- 885 Yu, R., Yang, Y., Yang, L., Han, G., & Move, O., 2016. RAQ—a random forest approach for
886 predicting air quality in urban sensing systems. *Sensors*, 16(1), 86.
- 887 Zhai, B., & Chen, J., 2018. Development of a stacked ensemble model for forecasting and
888 analyzing daily average PM_{2.5} concentrations in Beijing, China. *Sci. Total Environ.*, 635,
889 644-658.
- 890 Zhang L, & Singh V P., 2019. Copulas and their applications in water resources engineering.
891 Cambridge University Press.
- 892 Zhang, Y., 2017. Air quality modelling: Current status, major challenges and future prospects.
893 *Air Qual. Clim. Change*, 51(3), 41.
- 894 Zhang, Y., Lang, J., Cheng, S., Li, S., Zhou, Y., Chen, D., & Wang, H., 2018. Chemical
895 composition and sources of PM₁ and PM_{2.5} in Beijing in autumn. *Sci. Total Environ.*, 630,
896 72-82.
- 897 Zhu, S., Lian, X., Wei, L., Che, J., Shen, X., Yang, L. & Li, J., 2018. PM_{2.5} forecasting using
898 SVR with PSO-GSA algorithm based on CEEMD, GRNN and GCA considering
899 meteorological factors. *Atmos. Environ.*, 183, 20-32.
- 900 Zhou, Y., & Guo, S., 2014. Risk analysis for flood control operation of seasonal flood-limited
901 water level incorporating inflow forecasting error. *Hydrol. Sci. J.*, 59(5), 1006-1019.
- 902 Zhou, Y., Guo, S., Xu, C. Y., Chen, H., Guo, J., & Lin, K., 2016. Probabilistic prediction in
903 ungauged basins (PUB) based on regional parameter estimation and Bayesian model
904 averaging. *Hydrol. Res.*, 47(6), 1087-1103.
- 905 Zhou, Y., Chang, F. J., Chang, L. C., Kao, I. F., & Wang, Y. S., 2019a. Explore a deep
906 learning multi-output neural network for regional multi-step-ahead air quality forecasts. *J.*
907 *Clean. Prod.*, 209, 134-145.
- 908 Zhou, Y., Chang, F. J., Chang, L. C., Kao, I. F., Wang, Y. S., & Kang, C. C., 2019b.
909 Multi-output support vector machine for regional multi-step-ahead PM_{2.5} forecasting. *Sci.*
910 *Total Environ.*, 651, 230-240.